Hydrogen-Alpha Exploration with Light Intensity Observation Systems III

Final Science Report

Paige Arthur, Cooper Benson, Brandon Boiko, Ryan Cutter, Flor Gordivas, Kristen Hanslik, Rebecca Lidvall, and Dylan Richards

Nomenclature

ADCS	Attitude Control and Determination System
BOM	Bill of Materials
CDH	Command and Data Handling
COSGC	Colorado Space Grant Consortium
EPS	Electronic Power System
FBD	Functional Block Diagram
GPIO	General Purpose Input and Output
H-alpha	Hydrogen alpha
HASP	High Altitude Student Platform
HELIOS	Hydrogen-Alpha Exploration with Light Intensity Observation Systems

Contents

I Mission **3**
- A Overview . . . 3
- B Premise . . . 3
  - 1 High Altitude Balloon Observation . . . 3
  - 2 Photometry . . . 4
- C Requirements . . . 4

II Design **7**
- A General Overview . . . 7
- B Optics . . . 7
  - 1 ADCS Camera . . . 7
  - 2 Science Camera . . . 8
- C Structures . . . 9
- D Attitude Determination and Control System . . . 10
  - 1 Photodiode Arrays . . . 11
  - 2 Stepper Motors . . . 12
  - 3 Control Algorithm . . . 13
- E Electrical and Power System . . . 14
- F Command and Data Handling . . . 17
  - 1 Raspberry Pi . . . 17
  - 2 Gertduino . . . 20
- G Thermal . . . 20

III Results **21**
- A Optics Performance . . . 21
- B Structural Performance . . . 21
- C ADCS Performance . . . 21
  - 1 Failure Analysis . . . 24
- D EPS Performance . . . 24
  - 1 Changes from Proposal . . . 24
- E CDH Performance . . . 24
- F Thermal Performance . . . 25

IV Lessons Learned **27**
- A Optics . . . 27
- B Structures . . . 27
- C ADCS . . . 27
- D EPS . . . 28
- E CDH . . . 28
- F Thermal . . . 28

V Conclusion **28**

Appendices **30**
- Team Demographics . . . 30
- Structural Diagrams . . . 31

Acknowledgements **39**

References **39**

I. Mission

A. Overview

The mission of Hydrogen-Alpha (H-alpha) Exploration with Light Intensity Observation System III (HELIOS III) was to prove the viability of solar observation on a high altitude balloon platform by tracking the sun and taking images in the near hydrogen alpha light wavelength. HELIOS III was designed as a payload on the High Altitude Student Platform (HASP). The HELIOS III team designed, constructed, and tested an optics system to capture high resolution images of the sun in the near hydrogen alpha wavelength. The payload used an ADCS system to locate the sun and orient the optics system towards the sun on-board a HASP flight.

Mission Objectives:

1. Observe and capture images of the sun in hydrogen alpha wavelength using the optics system.
2. Design and implement an ADCS to locate the sun in the sky and orient the optics system towards the sun.
3. Prove the viability of high altitude balloon solar observation during a COSGC sponsored HASP flight.

B. Premise

1. High Altitude Balloon Observation

Currently, the majority of solar observations are performed using ground or orbit based telescopes. These two methods of observing the sun have several drawbacks. Ground observations face issues with interference from atmospheric filtering, effectively lowering the quality of solar images and reducing the ability to gather accurate scientific data from those images. Orbiting observatories are extremely expensive, limiting the quantity of such solar imaging missions in space. The lower quantity of orbital missions causes reduced access to the solar images taken by orbital observatories. With these restrictions in mind, an alternative method to observe the sun is through the use of high altitude balloon observatories. High altitude balloons are a relatively inexpensive platform. The HASP shall travel above 99.5% of Earth's atmosphere, mitigating the effect of atmospheric interference during solar observations.

The Colorado Space Grant Consortium at the University of Colorado at Boulder (CU) has a history of high altitude observatory experiments. DIEHARD (2008) determined the viability of high altitude observatories by collecting diurnal and nocturnal images of celestial bodies to determine atmospheric turbulence and light intensity due to residual particles in the atmosphere. This was done using photometers mounted 45-degrees from the horizon. BOWSER (2009) further determined the practicality of high altitude observatories by examining certain wavelengths of cosmic light and took corresponding diurnal images and light intensity readings of the sky. BOWSER also measured platform stability in order to determine the conditions in which future HASP missions will fly. SPARTAN-V (2010) worked towards the goal of supporting precise photometry from balloon based pointing systems and telescopes. SPARTAN-V focused on characterizing atmospheric scintillation and extinction to support the practicality of observing exoplanets from a high altitude balloon.

HELIOS III is the third iteration of the HELIOS mission. In 2012, HELIOS I began the mission to test the viability of solar observation on a high altitude balloon platform, but was not successful due to tracking issues caused by interference from the balloon and thermal failures of components in the EPS and CDH systems. In 2013, HELIOS II flew with the goal of improving upon the HELIOS I design. However, their mission was hindered by several issues. HELIOS III improved on the HELIOS II design by:

1. Adding baffles to mitigate bias in the tracking system due to reflections from the balloon
2. Improving the thermal properties of the payload to prevent overheating of components
3. Adding the ability to manually turn the system during flight

2. Photometry

The optics system captured images in near hydrogen alpha wavelength. What is considered visible light can be separated into two categories: light that is seen with the naked eye and appears in images as white light, or the filtered spectrum of this white light, which can be narrowed down to specific wavelengths. This filter system is used to observe details of the sun that would be obscured by the white light from the sun's photosphere.[4]

H-alpha filters allow the camera to detect only a small bandwidth of visible light around the wavelength of 656.28 nm. This wavelength is absorbed and re-emitted by the hydrogen in the suns atmosphere. It is one of the most useful wavelengths in which to observe the sun because it reduces the light from the photosphere, allowing high visibility of solar features. This interaction between emitted light and hydrogen in the sun's atmosphere predominantly highlights surface features.[4] Major solar features in this wavelength are solar prominences, sunspots, and coronal mass ejections. Therefore, H-alpha imaging of the sun provides incredible amounts of comprehensive data on solar activity.[2]

The atmosphere of the earth has shifting air pockets, which distort the view of ground telescopes despite scientific advancements in telescope design. The earth's atmosphere has a considerable amount of hydrogen, despite its small percentage of the total composition. This hydrogen also interferes with ground-based solar observation. New ground telescope technology has been able to correct for the atmospheric distortion to some extent but there is not a way of seeing the wavelengths blocked by the atmosphere. Solar observation will achieve the best clarity only if it is done above the atmosphere. HELIOS III ascended above 99.5% of Earth's atmosphere, which allowed the cameras to observe in these desired wavelengths without interference from the earth's atmosphere.[3]

C. Requirements

In order to complete all mission goals, the HELIOS III team followed all requirements specified by HASP in addition to all requirements derived from mission objectives. The HELIOS III requirements were as follows:

Level	Requirement	Derived
0	Hydrogen-Alpha Exploration with Light Intensity Observation System (HELIOS) III shall designed and constructed with an optics system for capturing images of the sun in the hydrogen alpha wavelength and utilizing an ADCS to locate the sun and orient the optics system towards the sun on-board a HASP flight	

Level	Requirement	Derived
0.1	Observe and capture images of the sun in hydrogen alpha wavelengths	0
0.2	Design and implement an ADCS to locate the sun and orient the optics system toward the sun	0
0.3	Design a high altitude balloon solar observation platform for a COSGC-sponsored HASP flight	0

Level	Requirement	Derived
0.1.1	The optics system shall implement an Hydrogen-Alpha filter allowing imaging of 656.28 nm wavelengths	0.1
0.1.2	The optics system shall implement a camera capable of gathering high resolution hydrogen alpha images	0.1
0.1.3	The CDH system shall allow for storage of captured images	0.1
0.1.4	One barrel of the optics system shall have a large field of view with low magnification	0.1
0.1.5	One barrel of the optics system shall have a small field of view with high magnification	0.1
0.1.6	The optics system shall be insulated and isolated from all other systems' thermal footprint	0.1

Level (cont.)	Requirement	Derived
0.1.7	The optics system cameras shall be compatible with the main CPU.	0.1

Level	Requirement	Derived
0.2.1	ADCS shall monitor changes of the sun's orientation along the elevation and azimuth	0.2
0.2.2	ADCS shall use motors to orient the optics system in the direction of the sun	0.2
0.2.3	ADCS shall be capable maintaining the sun within the field of view of the optics system	0.2
0.2.4	ADCS shall be designed with consideration to thermal effects on materials	0.2

Level	Requirement	Derived
0.3.1	HELIOS III shall comply with all HASP requirements outlined by the Call for Proposals and other LaSPACE documents	0.3
0.3.2	HELIOS III shall comply with all budget and schedule constraints dictated by COSGC and HASP	0.3
0.3.3	HELIOS III shall maintain a proper operational environment throughout flight	0.3

Level	Requirement	Derived
0.1.4.1	The optics system shall have one camera with a field of view no less than 15° x 10°	0.1.4

Level	Requirement	Derived
0.1.5.1	The optics system shall have one camera with a field of view of 1.5° x 1°	0.1.5
0.1.5.2	The optics system shall have one camera with a resolution of greater than 2500 pixels x 2000 pixels	0.1.5

Level	Requirement	Derived
0.1.6.1	The optics system shall remain below 60 °C throughout the flight	0.1.6

Level	Requirement	Derived
0.2.1.1	ADCS shall record sun's orientation in elevation every tenth of a second	0.2.1
0.2.1.2	ADCS shall record sun's orientation in azimuth every tenth of a second	0.2.1

Level	Requirement	Derived
0.2.2.1	ADCS motors shall be capable of rotating the optics system by 3° per second	0.2.2

Level	Requirement	Derived
0.2.3.1	ADCS elevation motor shall have a precision of at least 0.2° per step	0.2.3
0.2.3.2	ADCS azimuth motor shall have a precision of at least 0.04° per step	0.2.3

Level	Requirement	Derived
0.2.4.1	Azimuth and elevation motors shall remain below 60 °C throughout flight	0.2.4

Level	Requirement	Derived
0.3.1.1	Payload volume shall not exceed 38x30x30 cm	0.3.1
0.3.1.2	Payload shall resist the effects of up to 10 g vertical force and 5 g horizontal force	0.3.1
0.3.1.3	Payload shall utilize a twenty-pin EDAC 516 interface to HELIOS III system power and analog downlink channels	0.3.1
0.3.1.4	Payload shall not draw more than +30 VDC or 2.5 A and shall split the provided +30 VDC to voltages necessary to operate payload	0.3.1

Level (cont.)	Requirement	Derived
0.3.1.5	Payload shall enable six discreet command functions from HASP using EDAC 516-020 interface	0.3.1
0.3.1.6	Payload shall allow serial downlink functioning at 4800 baud	0.3.1
0.3.1.7	Serial up-link shall allow for 2 bytes per command	0.3.1
0.3.1.8	Payload shall use a DB9 connector, RS232 protocol, with pins 2, 3 and 5	0.3.1
0.3.1.9	Payload shall transmit payload status to the HASP serial downlink	0.3.1
0.3.1.10	Payload shall be mounted according to the HASP platform interface requirements	0.3.1

Level	Requirement	Derived
0.3.2.1	All receipts and proofs of purchase shall be retained	0.3.2
0.3.2.2	Schedule shall include weekly deadlines for each phase of design, assembly, and integration process	0.3.2
0.3.2.3	Schedule shall include all design document revisions; including relevant presentations	0.3.2
0.3.2.4	Schedule shall contain weekly team meetings	0.3.2

Level	Requirement	Derived
0.3.3.1	The optics system structure shall be insulated to minimize thermal footprint of other systems	0.3.3
0.3.3.2	All systems shall remain within operating temperatures while experiencing external temperatures between -80 to 60 °C	0.3.3

II. Design

A. General Overview

The payload was constructed of primarily of alluminum and consisted of a base housing and an upper housing. The base housing contained the main power board with the Raspberry Pi single board computer and the motor and gear that turn the payload in azimuth. The upper housing contained the two cameras. The motor and gear that turned the system in elevation were attached to the side of the upper housing. The payload used photodiodes to determine its position relative to the sun. One photodiode housing was attached to the side of the upper housing opposite the motor and the other was attached to the bottom of the upper housing. The base housing sits on a base plate to which many of the components heat sink. The functional block diagram of the system is illustrated in Figure 1. The full structure can be seen in Figure 25 on page 31.

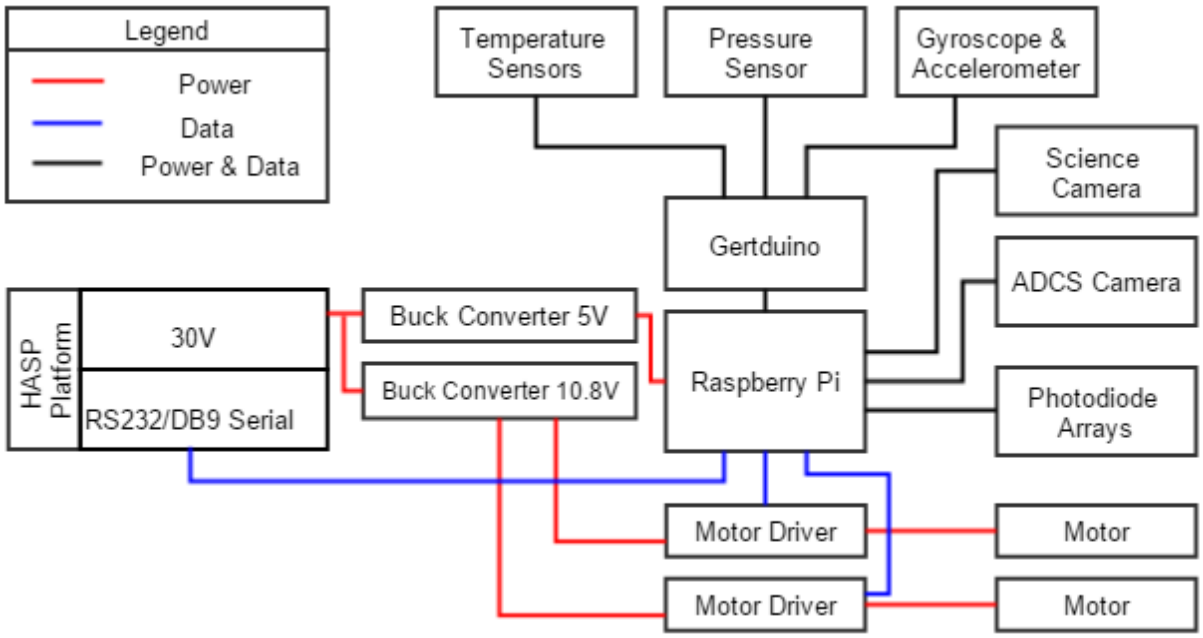

Figure 1: General FBD

B. Optics

The final design of the HELIOS III optics system was composed of two camera systems with two separate objectives. The ADCS camera system was designed to characterize the tracking system. The science camera system was designed to capture images of sunspots in the hydrogen alpha wavelength, while still being capable of capturing the entire disk of the sun. These two camera systems were mounted parallel to each other in the camera housing.

1. ADCS Camera

The purpose of flying the ADCS camera was to measure the performance of the sun tracking system. With a large field of view, the camera housing would only need to be pointed in the general direction of the sun in order to capture it. Photos from the ADCS team provided real-time visualization of how well the payload was tracking the sun. These ADCS photos could then be used to calibrate the photodiodes after flight. The ADCS camera is shown in Figure 2 on the following page.

The ADCS camera system used a DMK 42AUC03 camera that had a $\frac{1}{3}$ in. CMOS sensor chip with a 1280×960 pixel resolution, and a global shutter. In front of the camera was a camera lens with an adjustable 28mm aperture and two neutral density filters. The camera lens had a 12mm focal length and gave the ADCS

camera system the field of view of 22.9° × 17.2.° The sun's diameter is approximately 1.39×10^6 km and the earth is at an average distance of 1.496×10^8 km, away from the sun, resulting in an angular diameter of approximately 0.532° , or 1883″. This means the resulting picture on the CMOS chip would be 64.5 ″/px, or 47.583 km/px, based on the linear diameter of the sun being approximately 738.2 km/″. The resolution quality on the ADCS camera system was not of utmost importance. However it was important to ensure that the incoming light from the sun didn't damage the CMOS sensor chip. Therefore, there were two neutral density filters placed on the front of the camera lens that had different optical densities. The front neutral density filter had an optical density of 0.9OD and the filter behind it had an optical density of 3.0OD, which adds to 3.9OD. This equates to only 0.0122% of the light from the sun transmitting through the neutral density filters to the sensor. The filters were screwed into the front of the camera lens which was a standard C-mount thread.

2. Science Camera

The science camera was designed and flown with the objective of capturing images in the near hydrogen alpha wavelength in order to see sunspots on the surface of the sun. An image of the camera is shown in Figure 3. The HELIOS III team did not fly the telescope, or the concept, described in the proposal. Using the telescope design would have breached the HASP height limits. Instead, the science camera lens configuration from HELIOS II was flown with a few minor changes. The lens configuration was used in combination with the new DMK 51BU02 camera that had a $\frac{1}{1.8}$ CCD sensor chip with 1600 x 1200 pixel resolution and a global shutter. This camera, as opposed to the camera flown on HELIOS II, has a larger sensor chip providing a slightly larger field of view. The global shutter results in much less blur than a rolling shutter.

Figure 2: Photo of the ADCS Camera that flew; the neutral density filters are stacked on the right end

In front of the camera, is a C-mount tube, with a 25mm aperture, comprised of multiple pieces. The C-mount barrels were made of black anodized aluminum, which helped minimize outgassing, and were standard pieces that didnt need to be machined. The filters sat stacked in the rear piece, represented by the red piece in Figure 3, and the objective lens laid in the front piece, represented by the yellow piece. The filters sat in the rear piece in the following order: one dichroic longpass filter (purple), that filters UV light, one hot mirror (green), which filters IR light, and one narrow band-pass filter (red) with a 10nm bandwidth that passes light at 656nm (Hydrogen-Alpha filter)(Figure 3). The lens in the front piece was a single objective lens, placed and held by two retaining rings, with a 250mm focal length. The 250mm focal length was used to obtain the desired field of view of 1.95° x 1.56° .

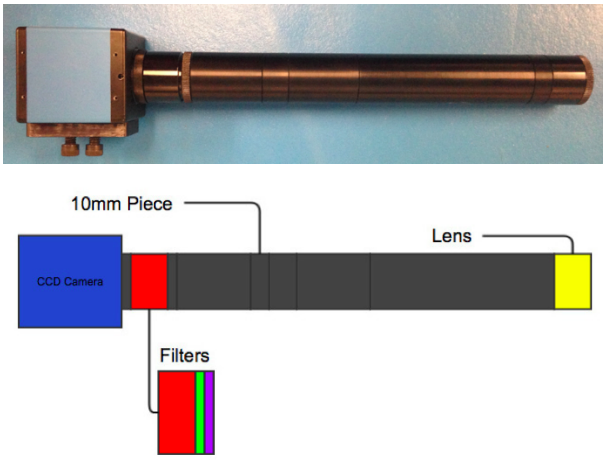

Figure 3: Picture and diagram of science camera; the total focal length of this system was approximately 255mm, including the 10mm piece

This field of view would ensure that the entire disk of the sun, the diameter being 0.5° , could be captured, without sacrificing magnification or resolution quality. Based on the same linear diameter of the sun as above, the science camera system achieved a plate scale of 3.63 ″/px, or 2679 km/px. However due to the 25mm aperture and 656nm wavelength, the diffraction limit is approximately 6.6″, or 4876 km, therefore the science camera system was oversampling slightly. This means that two features must be at least 4876 km away from each other on the surface of

the sun in order to be able to see a difference between the two features. The diameter of a sunspot can be anywhere from 16 km to 160,000 km, so the science camera system would be able to see any sunspots with a diameter larger than 4876 km.

C. Structures

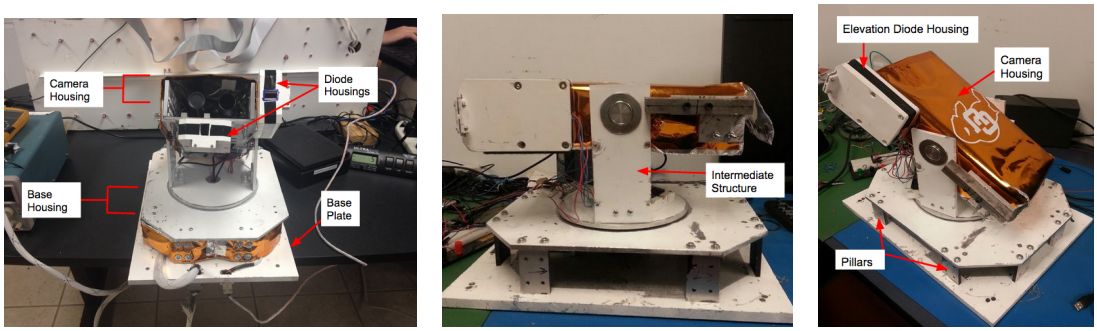

(a) Front of payload (b) Side of payload (c) Back of payload

Figure 4: View of Structure

The HELIOS III design consists of two major parts. The camera housing contains the optics system and comprises of the upper half of the structure. The base housing contains the components for EPS and CDH. The majority of the structure is made of 6061 Aluminum alloy. The proposed design contained a Maksutov-Cassegrain telescope; however, this required a larger camera housing than would fit inside the allowed envelope, since the height with the telescope implemented would have been 43 cm. As a result this design was rejected and a smaller refractive telescope was used, reducing the overall height of the system to 29 cm. The entire stucture is shown in Figure 5.

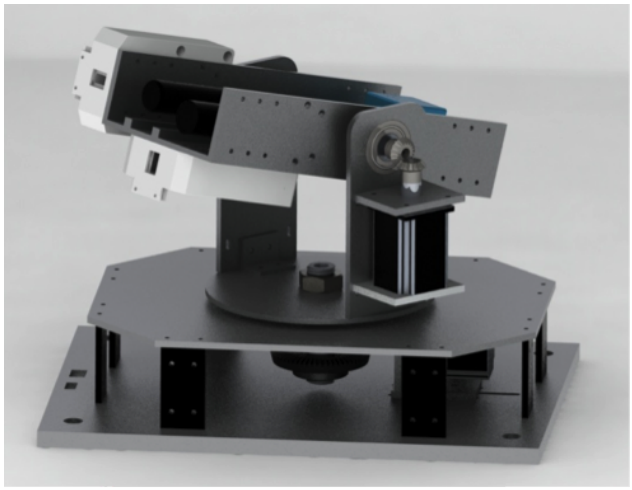

Figure 5: Full Structure

The base structure is shown in Figure 6a on the next page and consists of a base plate, a top plate, and pillars. It integrates directly to the HASP platform. The pillars support the top plate and the camera housing. An axle allowing rotation in azimuth is mounted directly to the top plate and is shown in Figure 7a on the following page.

The axle includes a gear, bearings, a flanged hub, and an aluminum tube. The gear connects to the azimuth motor, which is mounted on the base plate, through a 4:1 gear ratio. This ratio ensures enough torque to turn the camera housing in azimuth. This axle mounts to the top housing through holes on the flanged hub. Both the gear and the bearings are pressed onto the tube. Two bearings are used to minimize any wobble of the axle. A tube is used instead of a rod to allow wires to run to the camera housing through

the center of the axle. The axle is then pressed to a circular plate connecting the base housing to the camera housing. This is shown in Figure 7b.

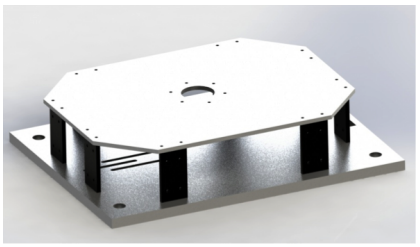

(a) Base Housing

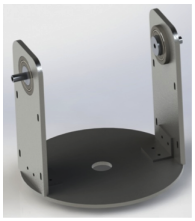

(b) Intermediate Structure

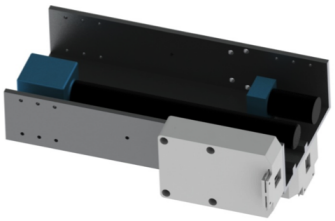

(c) Camera Housing

Figure 6: Structure

This circular plate is one of three parts to an intermediate structure consisting of the circular plate and two connecting arms (see Figure 6b). Bearings are pressed into each of the connecting arms to allow elevation rotation of the camera housing. A motor is mounted on the outside of one of the arms driving the elevation axle via a set of bevel gears. A gear ratio was not used here because it was thought that the system was already strong and precise enough to track the sun and it made finding the necessary components easier.

(a) Axle allowing for rotation on azimuth

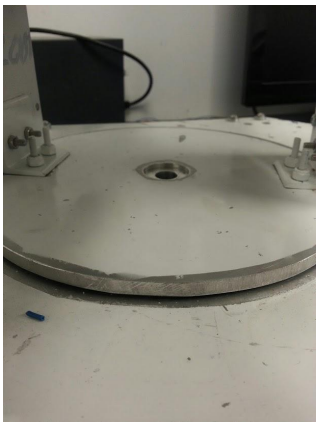

(b) Circular plate is pressed onto the azimuth axle.

Figure 7: Axle and Press-fit

One base plate and two side plates make up the camera housing, shown in Figure 6. The side plates connect to the elevation bearings through 1/4 - 20 screws which screw into dowels that are press fit into the bearings. Two photodiode housing are used, one for elevation, and one for azimuth. The elevation housing is mounted to the side plate, and the azimuth housing is mounted to the base of the camera housing. Multi-layer insulation blankets are used to cover the cameras, protecting them from the sun.

The photodiode housings are made of acrylic plastic. These housings are designed to contain multiple mounting holes, slots for photodiodes, razors, and filters. The housing is also baffled using a 30° viewing angle. The structure is shown in Figure 4 on the preceding page. Diagrams of the structure are shown in the appendix.

D. Attitude Determination and Control System

The primary task of the ADCS is to locate the sun in the sky and orient the camera housing towards the sun. Two photodiode arrays are attached to the camera housing. The array on the right of the camera housing detects the light along the y-axis or the elevation, while the array on the bottom of the camera housing detects the light along the x-axis or azimuth. Figure 8b on the next page illustrates movement along

elevation and azimuth. Figure 10a on the following page shows the positioning of the photodiode arrays relative to the camera housing. The Raspberry Pi micro-controller collects the photodiode readings and determines how far off from the sun the camera housing is. Then the Pi commands the stepper motors to move the camera housing. One motor moves the camera housing along the azimuth. The second motor was designed to move the camera housing along the elevation, but because of issues encountered immediately before flight, the second motor was not flown and the elevation was fixed at approximately 45° . The Pi commands the azimuth motor to rotate the camera housing until the photodiode and therefore the cameras are centered on the sun. The system tracks the sun constantly throughout flight to compensate for the rotation of the platform.

1. Photodiode Arrays

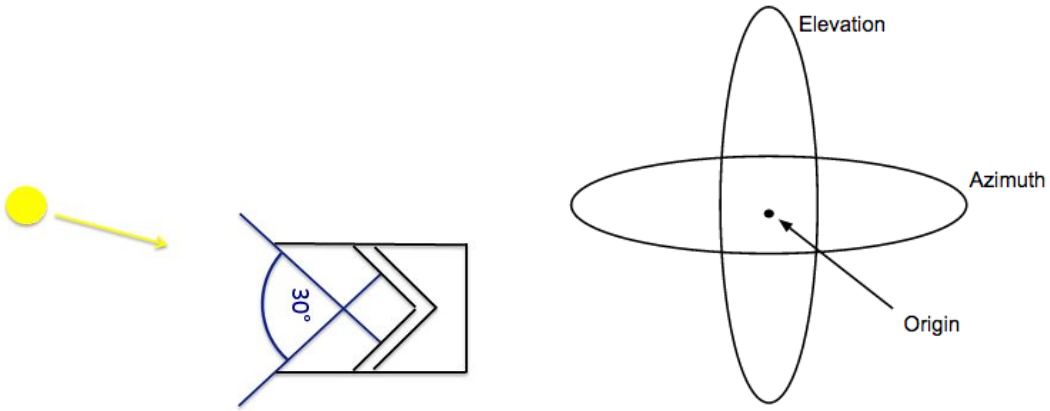

(a) Photodiode Housing Diagram

(b) Elevation and Azimuth

Photodiodes were used to measure light from the sun. The photodiodes output a current based on the amount of light measured by the sensor. As the light measured by the sensor increased, the photodiodes output more current. If no light was detected by the photodiodes, the photodiodes output a dark current. The dark current for the photodiodes was about 0.1 nA. The current output by the photodiode was very small, outputting a max current of about 0.04 µA. Because of this, the Pi was unable to read changes in the raw output signal. To compensate, the ADCS reverse biased the diodes by supplying 3.3 V backwards through them, which boosted the voltage across the two ends of the diode so that the Pi could easily read the difference. This was an easier solution than creating operational amplifiers, which would have required additional circuitry. With the reverse biasing, the photodiodes output 0 V in complete darkness and 3.3 V at full light saturation.

Two photodiode arrays were used in the ADCS. Figure 9 on the next page displays an image of the final photodiode array. One photodiode array was used to read light intensity on the azimuth, while the other array measured the light intensity on the elevation. Each photodiode array contained two small diode boards and each board contained two photodiodes, one primary diode and one backup diode, for a total of eight photodiodes in the system.

The housings were 3D printed in two separate pieces and are rectangular boxes. The inside of the housings creates a 90° angle at which the photodiodes are set. The geometry of the array is designed to maximize the ability of the photodiodes to track the sun. If the sun is in the center of the array, each photodiode in the pair reads the same light intensity. If the sun is off center but still in the field of view of the photodiode array, one photodiode reads a greater light intensity. The photodiodes are very sensitive to changes in angle. The photodiodes had a maximum sensitivity to angle changes at 45° from the normal. Based on the geometry of the array, when the sun was in the center of the array, it would be at a 45° angle from the photodiodes. Therefore, the diodes were positioned in the array so that they would be at their max sensitivity to change when the sun was near the center of the array. The housings were also built to baffle the photodiodes so that light reflected off the balloon or the platform would not skew the photodiode readings. Unfortunately,

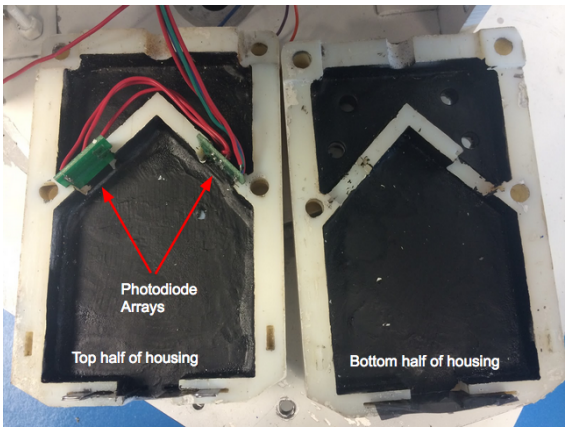

(a) Two halfs of photodiode housing

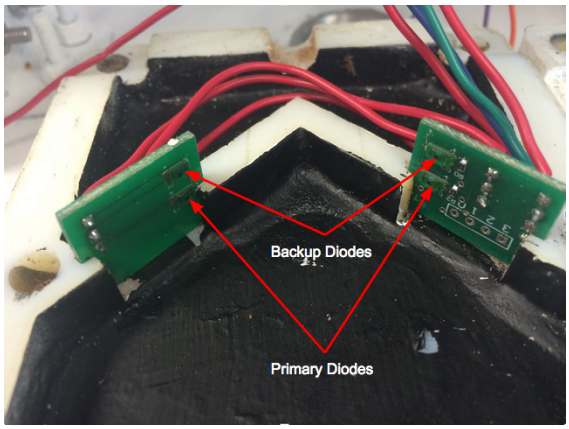

(b) Photodiodeiode Array

Figure 9: Inside of Photodiode Arrays

this also means that the field of view of the diodes is limited to approximately 30° in either direction. This is illustrated in Figure 8a on the preceding page.

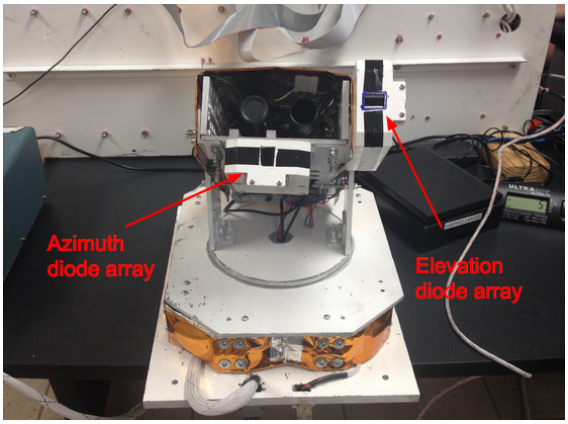

(a) Arrays relative to structure

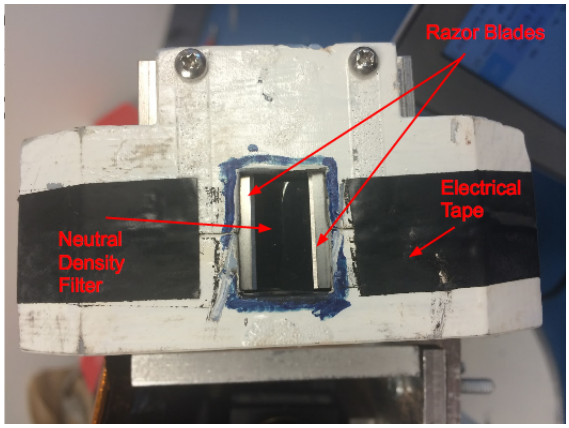

(b) Array showing filter, razor blades, and tape

Figure 10: Photodiode Arrays

When looking directly at the sun, the photodiodes would become saturated. In order to solve this problem, light diffusers were placed in front of the photodiodes. The light diffusers were neutral density filters cut to fit in the opening of the photodiode housings. The filters were Rosco E. Color Neutral Density Gels and blocked 75% of the incoming light, ensuring that the diodes did not become over saturated while still allowing for accurate readings. Furthermore, to compensate for any light reflecting off of the baffles, two razor blades were set at the opening of the diode housings. Electrical tape was placed around the junction of two halves of each housing to ensure that no extra light reached the diodes. This is illustrated in Figure 10b.

2. Stepper Motors

A stepper motor was used to move the camera housing by rotating it along the azimuth. The motor was bipolar motor with 200 steps per revolution that took 3.2 V at 2.8 A. An EasyDriver stepper motor driver was used to control the motor, and the Raspberry Pi microcontroller sent commands to the driver. The driver was used to power the motors and received 10.8V of power from the EPS board. The driver had a built in current limiter that was set at maximum to 750 mA. The basic setup is illustrated in Figure 11.

[a]Taken from: `https://www.sparkfun.com/products/10267`

The system was originally designed to have the same motor and motor driver turn the camera housing along elevation to up to 70° . However, since the driver only supplied 750 mA and the motor was designed to draw 2.8 A, the motors full holding torque of 19 kg-cm could not be achieved and the system was not strong enough to overcome gravity and turn the camera housing along elevation. This was also due to the fact that the heavy photodiode housings made the camera housing unbalanced and even more difficult for the motor to turn. As a result, the camera housing was fixed at an angle of approximately 45° for flight using a zip tie.

The driver allowed the motor to micro-step. Eight-step micro-stepping was used in the final design, allowing the motor could move 1600 steps per revolution. With the four to one gear ratio, the motor could move 6400 steps per revolution. This greatly increased the smoothness of the movement and allowed the system to point at the sun with an accuracy of 0.05625° . Since the field of view of the science camera was only 1.5° by 2° , a high degree of accuracy was needed to ensure that the sun could be captured in the images.

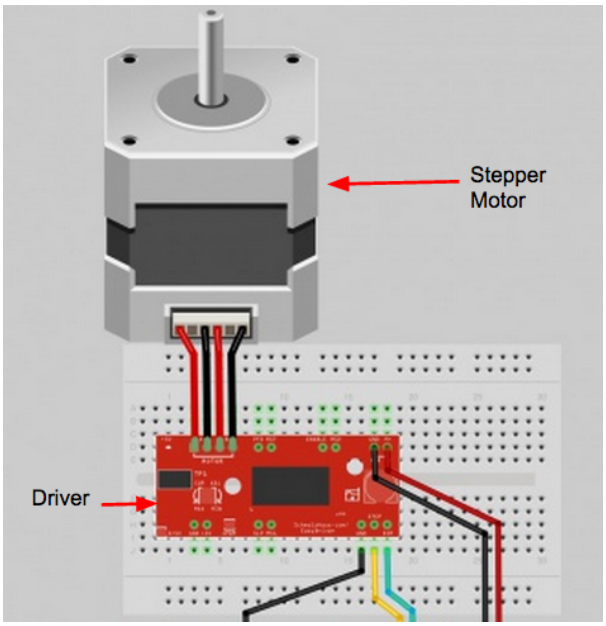

Figure 11: Stepper Motor and Driver [a]

3. Control Algorithm

The ADCS Control Algorithm consists of a single main flight loop, with several manual and automatic commands to respond to various situations encountered during flight. The ADCS system is controlled based on three data inputs: i) numerical readings from the azimuth diodes; ii) number of steps taken by the azimuth motor; and iii) live video data from the on-platform HASP live-streaming camera. These data sets are used to perform three different functions during flight: i) sun-tracking on azimuth; ii) resetting the azimuth location to zero; and iii) nudging on the azimuth to find the sun. Each of these functions was performed based on each of the three data sets, respectively. The control algorithm is illustrated graphically in Figure 12 on the following page.

a. Diode Readings and Sun-Tracking

Throughout flight, the two diode pairs collected data in the form of the voltage drop across the each diode. In order for the microcontroller to read these voltages, the diode outputs were run through Analog to Digital Converters (ADCs) , which returned signed 16 bit binary numbers, in the form of the difference in readings between the two diodes of a pair. Both azimuth and elevation readings were recorded, but only the azimuth diode readings were used as the ADCS system only tracked on azimuth. The readings were run through a moving average in order to smooth out the readings and minimize electrical interference and variability.

These averaged readings were what was used to track on the azimuth. If the readings were greater than a set tolerance value, the microcontroller would tell the motor driver to turn the motor one microstep in the clockwise direction. If the readings were lower than the negative of the set tolerance value, the microcontroller would tell the motor driver to turn the motor one microstep in the counterclockwise direction. Readings above the tolerance would correspond to the diode on the left of the azimuth diode housing reading greater than the one on the right, and therefore the sun being on the right of the payload when looking from the point of view of the payload. Readings below the tolerance would correspond to the opposite of readings above the tolerance.

The diodes constantly read voltage drop, and the ADCs had a sampling rate of 6 Hz. Therefore, the motor was able to turn one step every seventh of a second, as the motor was capable of turning one step for every diode reading. The tolerance value implemented in the controlling of the motor based on the diode readings was implemented because of the natural electrical noise and variation in the diode readings.

Had there been no tolerance, the housing would constantly move back and forth as the motor turned with changing diode readings. The tolerance allowed for the housing to not move when the diodes were centered on the sun within that tolerance.

b. Azimuth Motor Steps and Resetting the Azimuth Location

Throughout flight, each step that the azimuth motor took was recorded in a step count. This step count was constantly downlinked to the ground through the HASP platform. The step count was initialized at zero, and every time the motor took a step in the clockwise direction, the step count increased by 1. Likewise, every time the motor took a step in the counterclockwise direction the step count decreased by 1.

A full step for the motor corresponded to turning 1.8° . The motor driver was set to have the motor take eighth steps, corresponding to 0.225° per step. The azimuth motor system was connected to the top housing via a gear system with a 4:1 gear ratio. This gear ratio decreased the number of degrees taken per step by the magnitude of the ratio. Therefore, one step taken by the motor moved the camera housing by 0.05625° on the azimuth. This means that 360° or one revolution about the axis was equivalent to the motor taking 6400 steps in either direction.

Once the system stepped 360° in either direction, it would automatically turn back 360° to reset to the origin. This prevented the wires running from the base housing to the camera housing from getting tangled or pulling out of the components.

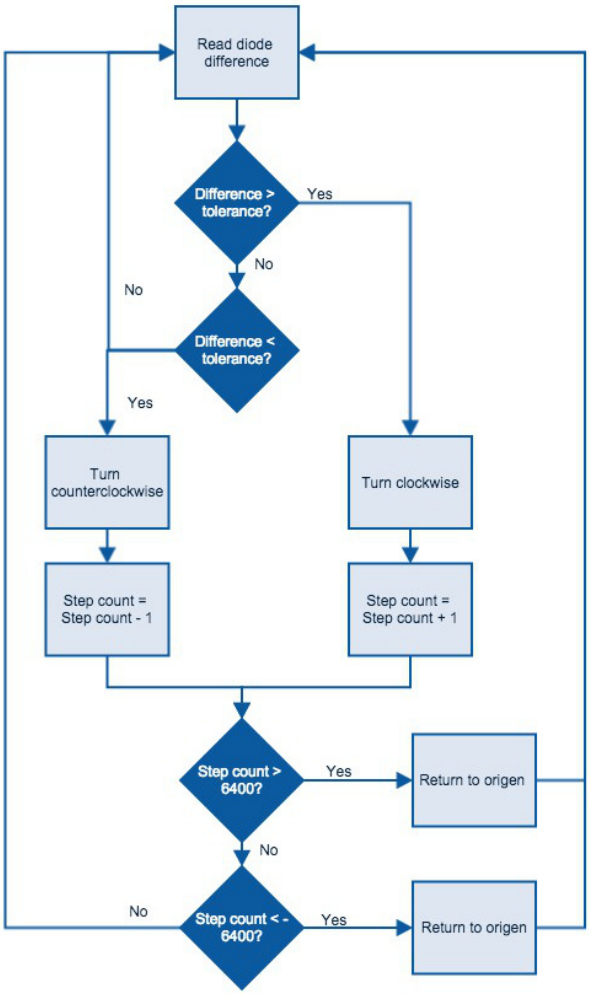

Figure 12: ADCS Algorithm

c. Live Video Data and Nudge Commands

During flight, the HASP Platform broadcasted a live feed from a video camera stationed on the ladder of the balloon above the platform. HELIOS III could be clearly seen from this video feed. The data received from this video feed is qualitative. Nudge commands were implemented that allowed the HELIOS III team to manually turn the platform at 10° or 90° intervals if they visually observed that the payload was pointing away from the sun. The use of the nudge command is discussed in the results section.

E. Electrical and Power System

The Electrical and Power System (EPS) focused on four main objectives to accomplish the HELIOS III mission:

1. To provide appropriate voltage and current to other subsystems
2. To monitor and adjust the power consumption of all components as necessary to protect the system To receive and transmit from sensors and other subsystems components
3. To ensure that the total electrical current pulled from the HASP platform did not exceed 2.5 Amps

These tasks were accomplished by designing a printed circuit board (PCB) which contained the essential components and routed power to the systems where needed. The flown power board is shown in Figure 13

The major components that were used to accomplish these tasks were a Raspberry Pi, a Gertduino, two buck converters, a USB Hub, and two motor drivers. Implemented in later designs were also current sensors and power switching mechanisms to control power consumption. The block diagram for the system can be seen in Figure 14 on the following page.

Power was provided to the HELIOS III payload by a twenty-pin EDAC 516 connector, with 4 lines of 30V. As this was too high of a voltage to run the components on the payload, the voltage needed to be stepped down to a lower level. A major consideration that influenced this implementation was thermal analysis. Because previous iterations of HELIOS had difficulties with the EPS system due to overheating, buck converters from V-Infinity were used. Although they were large, measuring 2.28 in by 2.40 in, they were very efficient components with a low risk of overheating or burning out. They were also connected to a part of the aluminum structure via a thermal conduction pad to help dissipate heat. For the Raspberry Pi, Gertduino, and USB hub, one buck converter stepped the 30V down to 5V. The motors that rotated the payload along the elevation and azimuth axes used an output voltage between 8-30V to the motor. This was achieved by using a 30V to 12V buck converter, and using the trim feature to bring the voltage to a desired 10.8V. To achieve the highest current possible, a small voltage was desired so 10.8V was used because it was the lowest that the voltage converter could output while still being in the motors range.

Component	Voltage (V)	Current (A)	Power Draw (W)
Raspberry Pi	5	1.1	5.5
Gertduino	5	0.5	2.5
Motor Driver 1	10.8	0.75	8.1
Motor Driver 2	10.8	0.75	8.1
USB Hub	5	2	10
		Total Power Draw	34.2

Table 2: EPS Power Budget

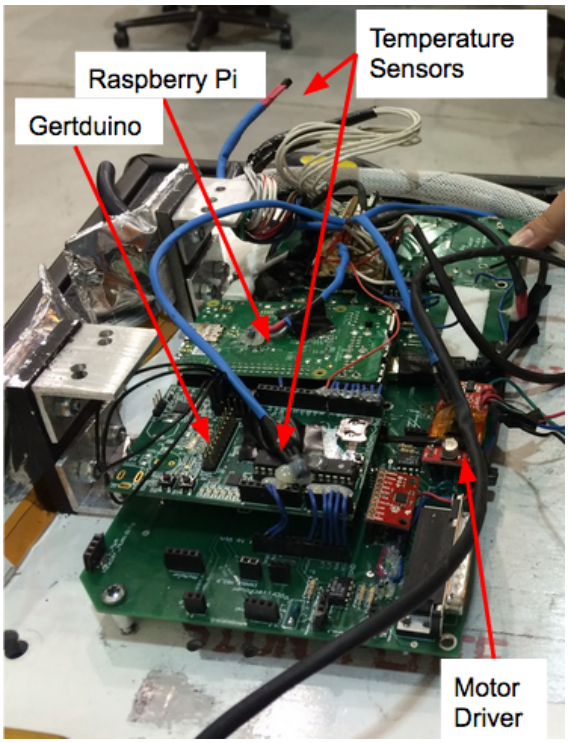

Figure 13: Flown power board

The Raspberry Pi and Gertduino handled the data collection and commands for the payload. Both microcontrollers were connected to the PCB in order to handle the routing to other components. Although they are designed to stack on top of each other, they were separated and the necessary connections between the two were made within the PCB in order to have access to some of the pins that otherwise were unusable.

The cameras communicated with the microcontrollers via a USB cable that was plugged directly into the Raspberry Pi to transmit data and receive power. However, because both cameras drew about 750mA of current and the current limit on the Raspberry Pi is 1.5A, having both cameras connected and running at once caused the Raspberry Pi to shut down and reset due to high current draw. To fix this problem, a USB Hub design was used. There are two connections on the USB Hub: one connects to the Raspberry Pi via USB cable for the data lines, and the other is a barrel jack that takes power from the 5V buck converter. This allowed for the data lines from the cameras to go to the Raspberry Pi while the power was drawn from the buck converters so the currently limit was not reached on the Raspberry Pi.

The motor drivers that controlled the elevation and azimuth motors were chosen by the ADCS team based on their requirements. Once chosen, the EPS team powered the motor drivers both with the logic lines from the Raspberry Pi that allowed the driver to perform as desired. The 10.8V lines that were used to drive the motors themselves were also controlled through the motor drivers on the PCB.

Lastly, the EPS board also supported environmental sensors including multiple temperature sensors, a pressure sensor, and a combined gyroscope and accelerometer. These sensors were used to make a profile of the flight as well as to assist in post flight analysis including thermal information to ensure that components did not overheat during flight.

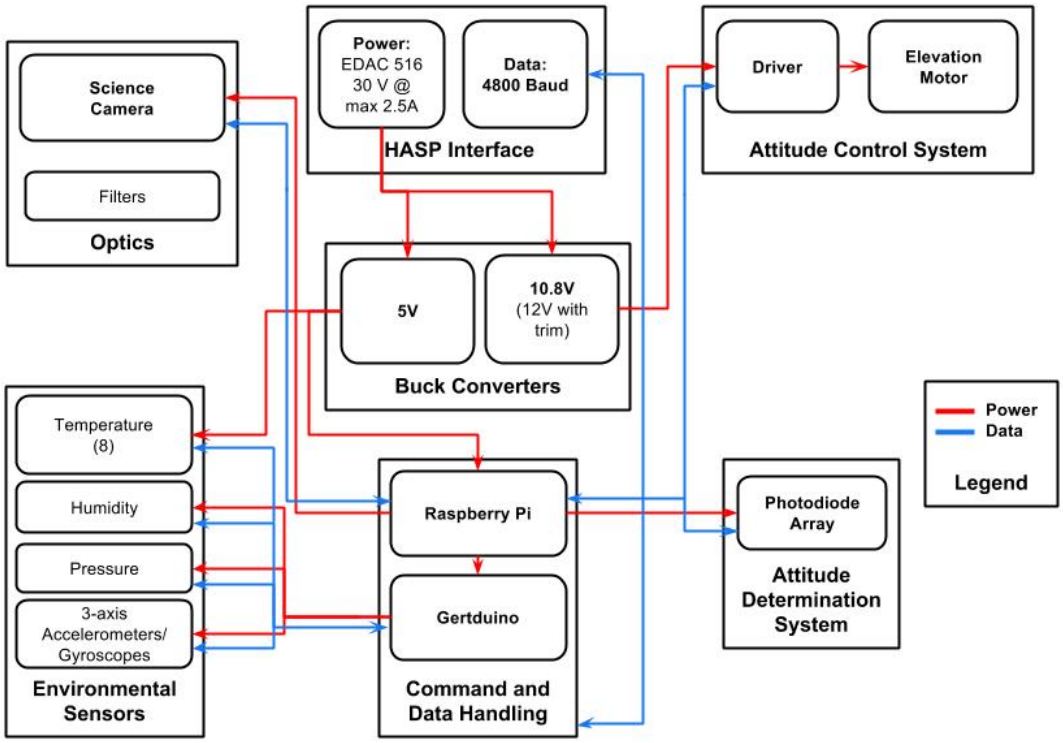

Figure 14: EPS FBD

As for the last goal of ensuring that the current drawn from the HASP platform did not exceed 2.5A, a power budget was calculated. This can be seen in Table 2 on the previous page. In order to make sure that the maximum current was under the limit, the values in the power budget are highest-draw scenarios where

the actual power drawn may be less. Since the total power draw was 34.2W and the voltage supplied from the platform was 30V, the maximum current draw was less than 1.25A.

F. Command and Data Handling

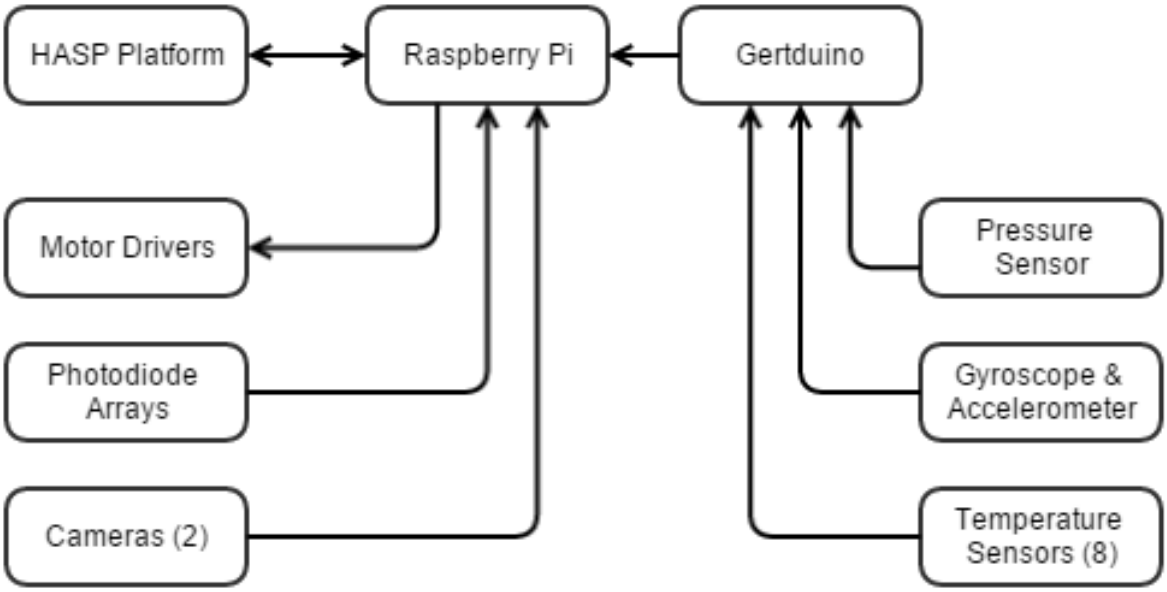

Figure 15: CDH FBD

The CDH system aboard HELIOS III was responsible for communications with the HASP platform and collecting and managing data from the Optics, EPS, and ADCS subsystems. As such, the design of CDH utilized a Raspberry Pi B+ microcontroller, Gertduino, and flight code written in C++ and Python. The Gertduino is a board similar to an Arduino Uno with an added microcontroller, RTC, and RS232 level controller, with the specific intent of being used to augment a Raspberry Pi. A FBD of the design can be seen in Figure 15.

1. Raspberry Pi

The Raspberry Pi (shown in Figure 16a on the next page) was the main component in the CDH design, controlling communications with the platform and Gertduino, capturing images, and supporting the ADCS subsystem. The Raspberry Pi was connected to the photodiode arrays and motor drivers and controlled sun tracking. It also was connected to the platform using a RS232 to USB converter and cameras using USB 2.0.

In order to handle this variety of goals, the Raspberry Pi ran flight software that was separated into 5 distinct threads. This allowed the threads to run concurrently on the processor without allowing one thread to monopolize the processor. The threads utilized locks and semaphores to prevent attempted concurrent use of the communication buses, files, or other single-actor resources, and passed data between them with queues. The threads are documented below, with the exception of the ADCS thread which is covered in Section D.

a. Monitoring Commands from Ground `uplk`

The uplk thread was responsible for awaiting two-byte serial commands uplinked by the ground station. It idled until it detected data in the serial buffer, then passed the relevant information to the threads affected. If any issues were detected with the uplinked command, it would downlink an error to ground. Table 3 on the following page documents the commands used by the HELIOS III team. Upon the execution of a

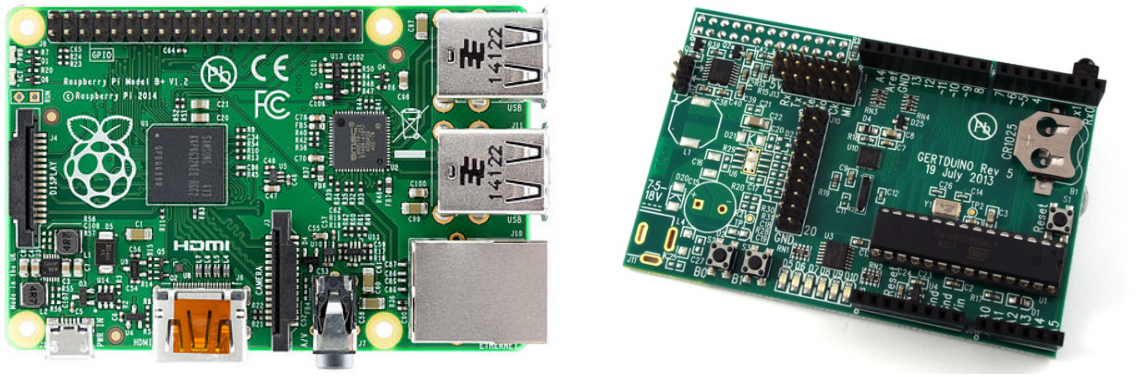

(a) Raspberry Pi (b) Gerduino

Figure 16: CDH Flight Hardware

command, the executing thread would downlink an acknowledgment. The thread would then idle until more data was uplinked to the payload.

Payload Command	Two Byte Hex Command	Description
Reinitialize Pi Program	0x0B 00	Causes the flight code to reset to known state
Pan mode on Pan mode off	0x0C FA 0x0C FB	Toggles panning mode for total diode failure
Toggle diode pair - phi Toggle diode pair - theta	0x0C 1A 0x0C 0A	Toggle between main and backup diodes
Clean Shutdown	0xFF FF	Allows clean shutdown of threads
Ping	0xAA AA	Ping the payload to test communications
Nudges	0x0C F0 0x0C F1 0x0C F2 0x0C F3	-10 Nudge 10 Nudge -90 Nudge 90 Nudge
Autopan	0x0C FC	10s Panning mode

Table 3: Command Table

b. Downlinking Data to Ground `dwnl`

This thread processed and downlinked data from the other threads to be sent to ground. It would idle until a thread passed it a data package containing the identifier of the author thread, the record type, and data. The downlink thread would then format the information into the downlink format, documented in Table 4 on the next page, along with the types of downlinked packages. The goal of the downlink format was to easily identify any data loss or corruption, and allow for easy sorting.

c. Communicating with the Gertduino and Capturing Images `gert` *and* `capt`

The gert thread was responsible for gathering information from the Gertduino and downlinking it to ground and was intended to forward commands to the Gertduino. There were no actual commands assigned to

Bytes	Content	Example
0-4	Start	STX
5-7	Payload Identifier	CU
8-10	Thread Identifier*	PI
11-13	Record Type*	AP
14-18	Timestamp	1400019944
19-22	Length of data	37
23-26	Adler32 Checksum	-71889546
27	New line	STX
28-(N-4)	Data*	The red fox jumped over the brown log.
(N-3)-N	End Transmission	XTX

Sender	ID	Record	ID	Content	Typical Data
Uplink	UP	Bootup	BU		0xBB
		Ack	AC	Responding to ping	
		Error	ER	Invalid target	<2 bytes>
Downlink	DW	Bootup	BU		0xBB
Gertduino	GE	Bootup	BU		0xBB
		Downlink	DW	Data	Data Package
ADCS	AD	Bootup	BU		0xBB
		Ack	AC	Command executed	<1 byte>
		Error	ER	Command with error	<1 byte>

Table 4: Data downlink format

the Gertduino (see part 2), so it solely forwarded environmental data from the Gertduino to the downlink thread.

Capt was a thread that took a picture from the science camera and stored it at approximately a rate of 12 per minute. It would capture an image, convert it to a grayscale PNG, save it to disk, pause one second, and repeat. A more complicated system was intended, that would intelligently capture images when the sun was close to being in frame, but was not implemented.

2. Gertduino

The Gertduino (shown in Figure 16b on page 18) was responsible for collecting environmental data and passing it on to the Raspberry Pi, and was intended to control power to components if they were over their temperature or current limits. This feature had to be removed due to issues both with the power switching itself (see EPS discussion of failure) and the serial communications link with the Raspberry Pi.

It was connected to a pressure sensor, accelerometer, gyroscope, and eight temperature sensors. It would collect data from these sensors every 5 seconds and forward the information to the Raspberry Pi via the serial connection. It also housed the RTC which the Raspberry Pi used to set its internal clock when it was powered off. This allowed for consistent time keeping between the various boot-ups of the Raspberry Pi, allowing for easy determination of what data was from flight and which was not.

G. Thermal

To prevent components from malfunctioning due to temperatures reaching outside their optimal working range, a simple thermal system was implemented. To prevent the EPS buck converters from overheating, a half inch aluminum 6061 baseplate was used as a heat sink. As the standard baseplate supplied by HASP cannot perform as an effective heat sink, an aluminum 6061 baseplate was constructed to replace it due to its relatively high heat capacity. To interface and ensure greater thermal conductivity between the baseplate and the Buck Converters, Tflex thermal gap filler of 0.508 mm thick with a thermal conductivity of 5.0 W/(m K) was used. This is shown in Figure 17.

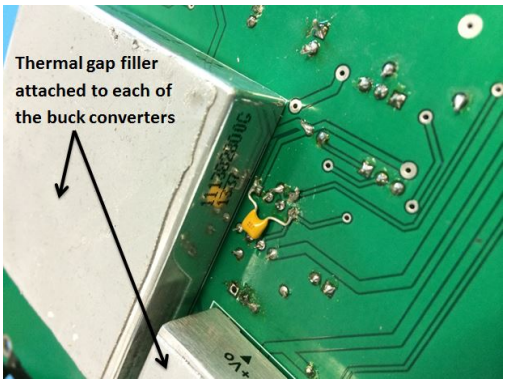

(a) Buck Converters with a thermal gap filler

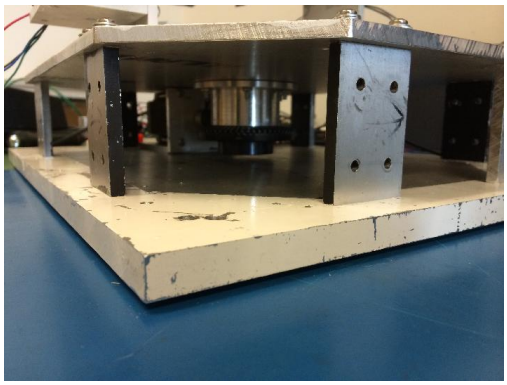

(b) Aluminum 6061 baseplate heat sink

Figure 17: Heat Sinking

To minimize contribution of heat from the sun, MLI was used around the upper part of the structure that contains the cameras as well as around the outer perimeter of the base structure. To prevent the structure from absorbing as much external heat as possible, the additional metal surfaces exposed to the sun were sprayed with white appliance paint which has a relatively high emissivity to absorbance ratio. The inside of the pillars were painted black to ensure a high absorptivity to emissivity ratio. To characterize the performance of this thermal system, eight temperature sensors were used to monitor components, baseplate temperature, and ambient temperatures.

III. Results

A. Optics Performance

Unfortunately, due to problems and complications encountered at integration, the HELIOS III team was not able to fly a functioning ADCS camera system. HELIOS III did fly the science camera system and was able to successfully capture part of the sun in 75 pictures, two of which are shown in Figure 18.

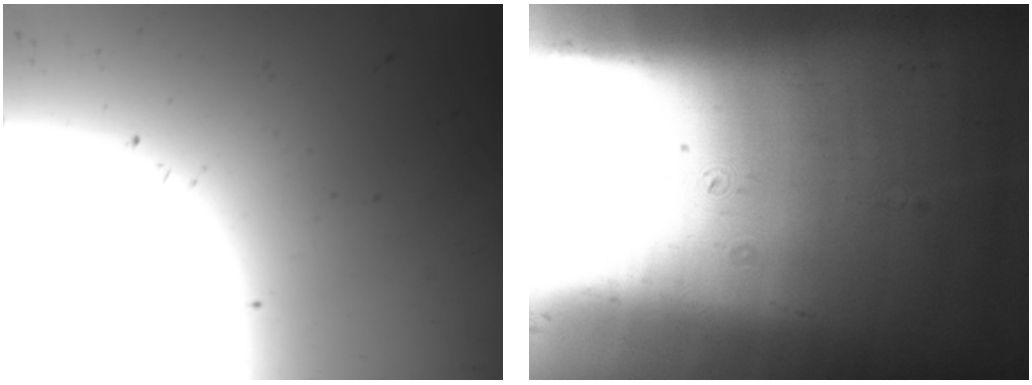

Figure 18: Science Images

The science camera system was set to take photos with a one second pause during the entire flight, resulting in over 6,000 total photos with 1.19% of them containing the sun. However prior to launch, the camera housing had to be set to a fixed elevation due to problems encountered at integration, which resulted in a single approximately 10 minute window in which the sun was at a high enough elevation in the sky to be seen by the science camera system. The science camera system was able to capture the sun in 50% of the photos taken during that 10-minute window. The photos in Figure 18 are examples of some of the best photos from the HELIOS III flight. None of the photos captured the entire disk of the sun and the photos were too oversaturated to be able to view sunspots.

B. Structural Performance

The structure performed as expected during flight despite that the camera housing had to be set to a fixed elevation. While the camera housing was able to turn in azimuth, insufficient torque prevented it from turning in elevation. On impact the press fit between the axle and the circular connecting plate became separated but no internal or external components were damaged. The structure was in two pieces for recovery, the base structure, and the camera housing mounted to the intermediate structure.

C. ADCS Performance

By visually observing the payload through the live feed camera, it could be seen that the system tracked well throughout the entirety of flight. The only times that the system did not seem to be pointing the general direction of the sun occurred when the sun was very low or very high in the sky or when the platform was in the shadow of the balloon. The nudge command was used once during flight when the system was pointing too far away from the sun to have it in its field of view. The command behaved as expecetd, turning the payload ten° at which point the payload was one again able to track the sun.

The science camera captured 6,227 images during flight. 75 of these images contained at least part of the sun, and even more images contained light that was most likely but not certainly the sun. The percent of images containing the sun was 1.19%. Considering that the system had a limited tracking window due to that the ADCS camera was not flown and that the elevation was fixed at a set angle, this percentage is relatively high. In fact, approximately half of the images taken during the tracking window contained the sun.

In images containing the sun, the sun is located in the left side of the image. No picture contains the entire disk of the sun. This is due to inaccurate calibration of diodes prior to flight. That the sun varies in location from the bottom of the image to the top of the image is indicative of the fact that the elevation was

fixed at a set angle. Therefore, the sun started in the bottom corner of the field of view and moved upwards until it passed out of the top corner of the field of view. This progression can be seen in Figure 19.

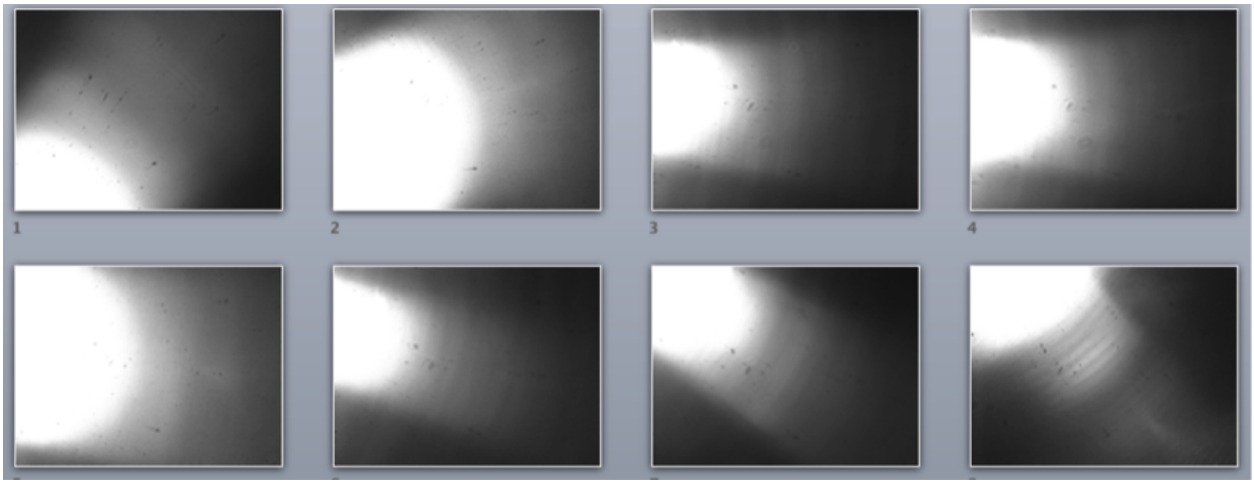

Figure 19: Progression of sun into and out of the science camera's field of view

Figure 20a on the next page shows the movement of the upper housing in azimuth over time throughout the duration of flight by displaying the step count of the motor. The step count was initialized at zero, and for each step in the clockwise direction the step count increased by 1. Likewise, for each step in the counterclockwise direction the step count decreased by 1. Horizontal sections of the plot represent zero movement in azimuth. As evidenced by the step count registering zero, the upper housing stayed stationary at its original position until the platform reached float (marked by the vertical green line). The upper housing rotated in azimuth, tracking the sun as the platform rotated. The plot has horizontal lines at ± 6400 steps denoting the maximum steps allowed in either direction. Throughout flight the upper housing turned 360° in one direction and subsequently reset to its original location on four separate occasions. This is visible in the plot when the step count reaches 6400 and quickly drops back down to zero. When observing the step count throughout flight, it is clear that the payload was almost constantly moving. This is expected, as the balloon platform rotated back and forth on its azimuth. The tracking system compensated for this movement by moving in the opposite direction in order to stay centered on the sun.

Figure 20b on the following page is a plot of the elevation diode readings throughout flight. The vertical green line represents launch.

Because the payload was fixed on the elevation axis, the sun was only in the field of view of the elevation diodes for a short time, approximately 30 minutes. As shown by the plot, the difference in the diode readings increased dramatically as the sun transitioned into and out of the field of view. First the diodes read a positive difference as the sun entered the field of view from the bottom and the upper elevation diode was exposed to more light. Then the diodes read equal when the sun was in the middle of the field of view of the elevation diode array. As the sun moved upwards out of the elevation diodes field of view, there was a large negative difference in the diode readings as the lower diode was exposed to more light.

The period between these two regions of large diode differences was the optimal time for taking science images as this was when the sun was in the field of view of the diodes. The time when a science picture first contains the sun and the time a science picture last contains the sun are plotted on the diode graph, and the range between them falls directly between when the sun entered and left the elevation diodes field of view. Towards the end of the flight, the plot shows the difference in the diodes becoming more and more negative. This corresponds to the sun beginning to enter the field of view of the elevation diodes again as it was setting. During this time, the sun moved lower in the sky and was approaching an optimal position within the diodes' field of view. Unfortunately, flight was terminated before the sun re-entered the center of the diodes' field of view and more images could be taken.

Figure 20c on the next page is a plot of the azimuth diode readings throughout flight. The vertical green line represents launch. As evidenced by the plot, the azimuth diodes consistently read a difference at or near 0, indicating that the diodes were constantly focused on the sun. This demonstrates that the azimuth tracking system was highly successful. There were two spikes of difference in diode readings about 140 minutes into

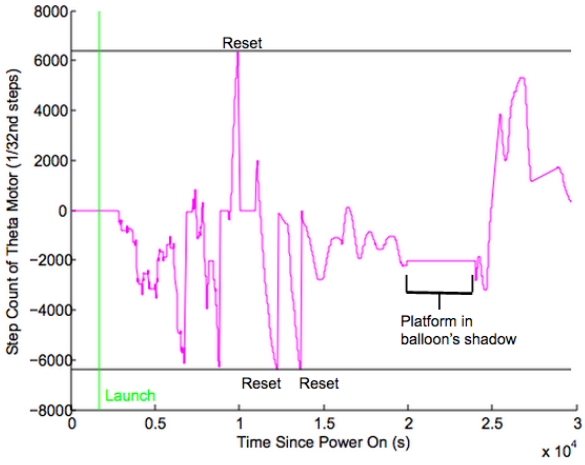

(a) Motor Step Count

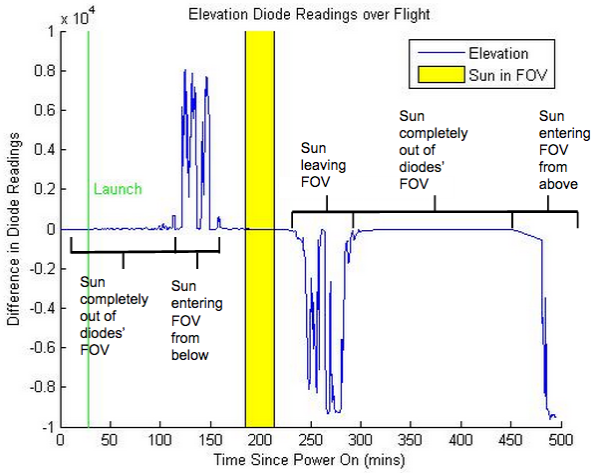

(b) Elevation Diode Readings

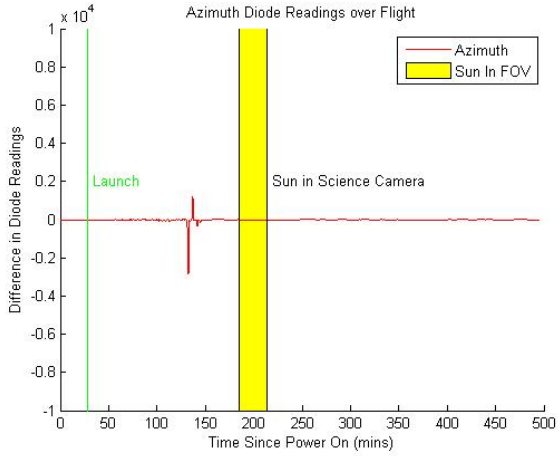

(c) Azimuth Diode Readings

Figure 20: ADCS Data

flight, corresponding to a possible reflection of light into the diodes or a shadow. However, these spikes lasted only seconds and subsequently did not affect the ability of the system to track the sun. With the exception of these two spikes, the azimuth diodes never read a difference greater than their calibrated tolerance. Reading a difference of within the tolerance means that the diodes were either both reading equal because they were focused on the black of space, or both reading equal because they were centered on the sun. By overlaying on this diode plot the times when pictures of the sun were taken, it is determined that the diodes were reading equal because they were centered on the sun, as there was a difference of zero when pictures of the sun were taken.

1. Failure Analysis

The ADCS System had partial success throughout the mission. Failure was primarily due to two factors. The first was that the elevation was set at a fixed angle, so the system could not track along elevation. The second was that the calibration on the azimuth diodes was slightly off, so the sun was too far to the left in captured images. Because only about half of the sun is visible in the best images, it can be concluded that the system was miscalibrated by approximatly a quarter of a degree.

D. EPS Performance

1. Changes from Proposal

The final flight EPS design was very different than what was proposed. These changes were mainly due to complications during integration. The power switching was not implemented, the USB hub design was changed, and only the science camera was flown.

a. MOSFETs and Power Switching

There were repeated failures of Raspberry Pi's connected to the EPS board caused by voltages over 3.3V being applied to the GPIO pins. This was traced to the motor drivers and was being caused the power switching method. It was designed to switch power on the low side using N-channel MOSFETs which resulted in the motor drivers inputting 10.8 V to the digital pins when the drivers were not connected to ground. As a temporary solution, the switching mechanism was removed by connecting the motor drivers directly to ground.

b. The USB Hub

The plan to use a USB Hub had to be redesigned when a short circuit rendered the hub useless prior to flight. As a solution to this, a USB cable was cut and the data lines were soldered directly into the board where they would have connected from the Hub. Two more wires were used to route 5V and ground to the cameras. This ultimately did not work due to mismatched voltages between the Pi and EPS board and contributed to the ADCS camera not being flown. Since only one camera can be plugged into the Pi without external power, the inability to power the cameras from the board only allowed one camera to operate during flight.

Other than these changes, the EPS board performed as designed during flight. Temperature data was gathered from multiple locations on the payload during flight and remained nominal throughout flight. The azimuth motor turned the payload to follow the sun when it was in the correct elevation range. The Gertduino and the Raspberry Pi were powered correctly and thus were able to gather and save data through out flight.

E. CDH Performance

During flight, CDH performed as expected. Flight status was monitored remotely from Boulder and commands were forwarded to the platform using Skype. Two commands were sent, acted upon, and acknowledged, and the Pi and Gertduino ran the entirety of flight without any outages. The payload downlinked 24941 data packets to ground totaling 1.3 kB of information, with a 2.71% corruption rate. The data corruption was due to an unidentified error with the HASP platform data downlink close to the end of flight. The checksums in the downlink packet allowed this data to be ignored during analysis.

The Pi also recorded 6,227 pictures for a total of 2.55 GB, which was substantially under the 20 GB picture estimate. This happened because most of the pictures were completely black and required little storage space after compression. There was an issue with images being only partially stored (see Figure 21). The reason for this has not been yet precisely identified, but there is a possibility that the capture code or PNG library used did not correctly handle file system errors or an error with the camera only sending partial images or being interrupted during transfer to the Pi. This is still being examined with the help of the camera manufacturer and extensive testing.

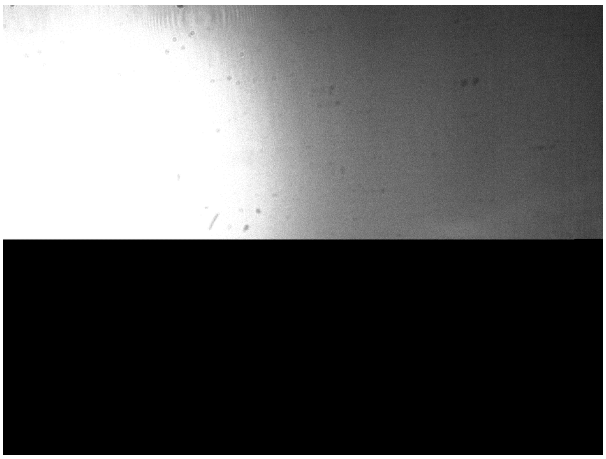

Figure 21: Partial Image

A processor fault also resulted in the ADCS camera not being flown. During integration, it was discovered that the Pi could capture images from the science camera but was not communicating correctly with the ADCS camera. This was caused by miscompiled camera drivers, caused by a problem in the operating systems compiler. This was not solvable without a full re-install of the operating system, which was not feasible given the late discovery of the problem and incomplete backups of the flight system.

F. Thermal Performance

During flight, no component met or exceeded its maximum operational temperature limit, illustrating that the thermal system performed successfully and that all components remained operable. The motor driver reached the highest temperature recorded on the payload, 77 °C, which is well below its maximum operational temperature of 135 °C. It should be noted that upon receiving the payload back after flight, most if not all temperature sensors were either not in contact with their respective component or only partially touching. It is not known if this loss of contact occurred before, during, or after flight and therefore implies that this data may not be depended on to present an accurate characterization of the payloads thermal performance. Looking at Figure 22 on the next page it can be noted that when the sun reached an elevation where the payload was blocked from the sun by the balloon, the temperatures all dropped. More interestingly, every temperature reading that measured temperature of a component had a decrease in temperature with much smaller slope than those that were ambient, internal, and external. A steeper slope and therefore quicker decrease in ambient internal and external temperatures indicates that while the ambient temperatures cooled off quickly when the sun went above the balloon, the components retained some of their heat and therefore cooled off slower. That this difference can be seen implies that the temperature readings are at least somewhat dependable.

To help characterize the performance of the baseplate as a heat sink the temperature of the baseplate was monitored. It is not certain which of three temperature sensors was monitoring the the baseplate as is depicted in Figure 22 on the following page. This is not known because these sensors were not labeled clearly in the data collected. However, as one temperature sensor was monitoring baseplate temperature, one of these three sets of data corresponds to that sensor. To compare the temperature of the baseplate to other temperatures, the sensor data with the highest overall average recorded temperatures was used. In Figure 23 on the next page it can be noticed that the temperature of the baseplate throughout the duration of the flight does not reach significantly high temperatures. In conclusion, due to the lack of overheating of any components it can be said that the thermal system worked as well as was necessary to maintain the thermal health of the payload.

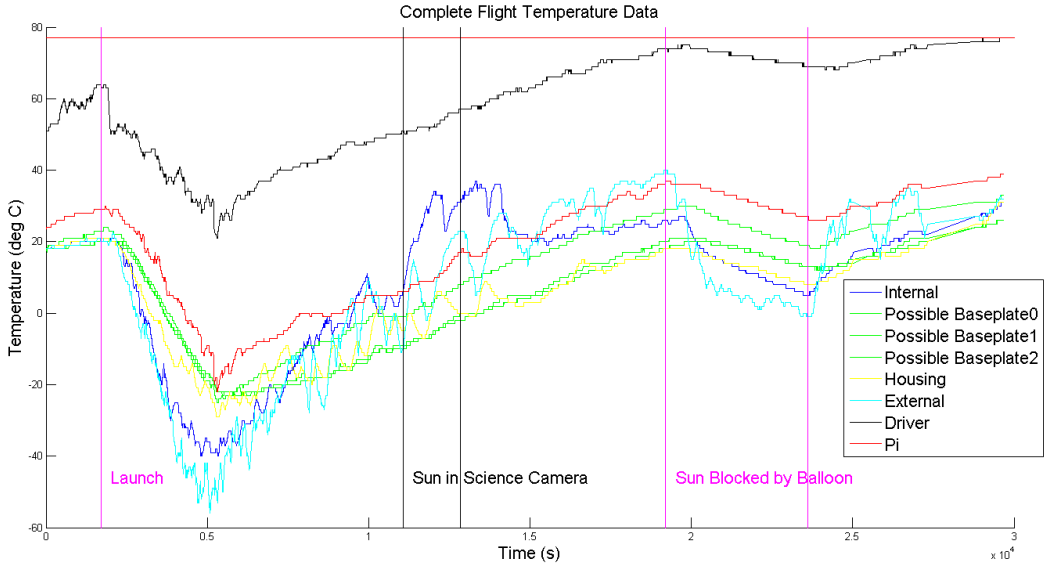

Figure 22: Temperature Sensor Data

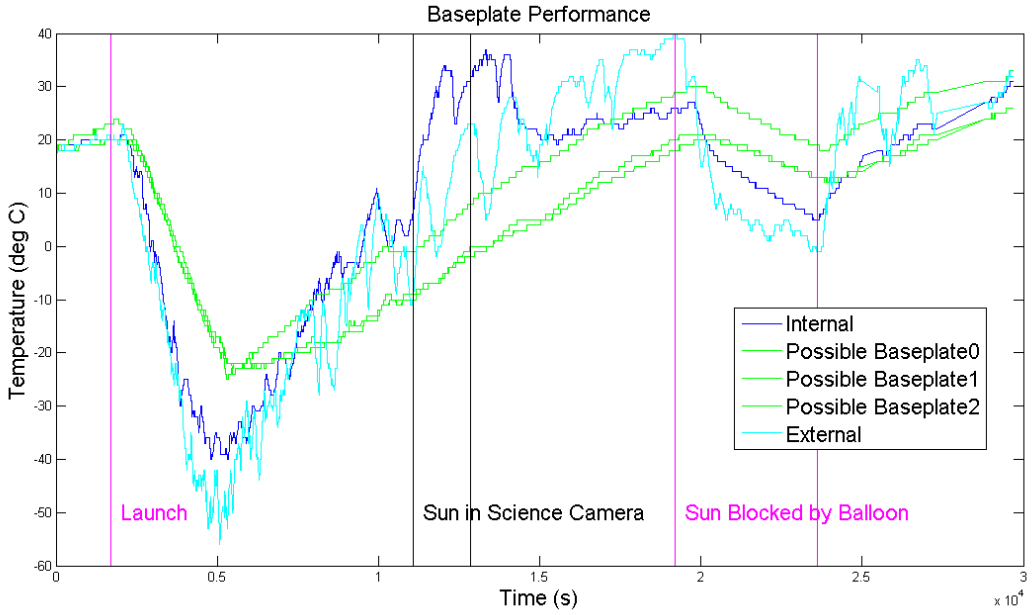

Figure 23: Baseplate Temperature

IV. Lessons Learned

A. Optics

The saturation of light in the photos could be attributed to a few possible factors. It is possible that the Gain/Gamma settings on the camera that adjust brightness were reset before flight. Having wrongly set Gain/Gamma settings would certainly cause too much light to be collected. It was also discovered that the length of the length of the C-mount barrel for the science camera system was actually 255mm instead of the desired 250mm. This is most likely because the lens was placed 5mm into the end piece, measuring 250mm to the end of the barrel. However, the camera sensor chip lies approximately 7mm into the camera meaning that the actual focal length of the system was approximately 7mm off from the focal length of the objective lens, thus out of focus.

To fix this problem, the 10mm piece was removed and an additional 5mm extender has been added behind the filters (see Figure 24). The total length of the new barrel is 250mm, and the objective lens will be screwed in 7mm from the end to offset the 7mm depth of the CCD sensor chip.

The camera system being out of focus would've contributed to the over saturation and glare seen in the results. A focused image would have a crisp, white disk in which the surface of the sun would be easily identifiable. To reduce the light intensity of the photos, additional filters would need to be implemented; specifically, a 5.0OD black polymer solar filter that will be placed in front of the objective lens. This filter will reduce the light intensity across the more than just visible light. The solar filter in combination with the currently implemented filters should produce a focused image in which sunspots are visible.

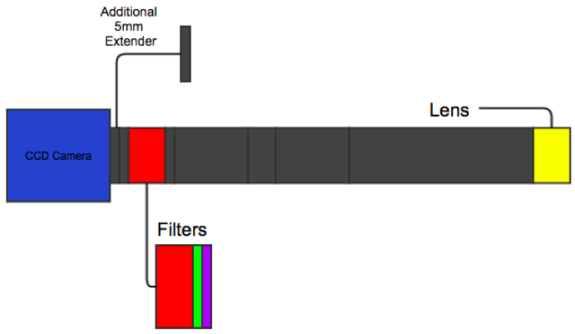

Figure 24: Diagram of the updated Science Camera system; the 10mm piece has been removed, and an additional 5mm extender has been added; the focal length of this new system is 250mm.

B. Structures

To improve the performance of the structure, some changes could be made. For one the structure was primarily assembled using brackets, nuts, and bolts. This led to a very bulky structure that was difficult to assemble and disassemble when necessary. This wasted time as we needed to constantly disassemble and reassemble the structure for repairs and testing.

The camera housing was also unbalanced which placed unnecessary strain upon the motors. More care must be taken to balance the housing while minimizing the amount of counterweights added.

The press fit for the azimuth gear created difficulties with alignment because it was hard to adjust the contact ratio for a smoother rotation. A gear ratio should have been used for the elevation motor in order to provide the torque needed to turn the camera housing.

The weak connection with the circular connecting plate may have been solved with a longer axle to provide more area for the fit. However for future reference a press fit should not be used to interface the camera housing with the base housing. Instead an OD thread would be sufficient to hold the circular plate whilst leaving room for wires to run through.

The two major lessons for designing a structure is to thread holes for assembly and to design without the need for a press fit. Threading holes will free up space by removing brackets, as well as make assembly easier. Press fits should only be used in structures when they are absolutely necessary. Significantly more time should have been spent on the design process for the structure, this would allow for all the major and minor issues to be worked out before expensive and time consuming machining takes place.

C. ADCS

The ADCS team learned that motors and motor drivers need to be chosen with more care to ensure that they are compatible enough to supply the motor with adequate torque. If this had happened, the elevation

motor would have strong enough to turn the system and the system would not have had to be fixed at an angle, increasing the time during which the sun has the potential of being in the camera's field of view.

Furthermore, the team should have spent more time calibrating the diodes. The fact that the sun was always in the left corner of the images is indicative that the diodes were calibrated slightly inaccurately.

The team also learned that the problem of reflections from the balloon faced by HELIOS II could be resolved by baffling the photodiode housings to a field of view of 30° . This prevented stray light from skewing the diode data without making it too difficult for the system to locate the sun. With the addition of several nudge commands to manually turn the system to face the sun if the system was ever facing the entirely wrong direction, the system never had any trouble finding the sun.

D. EPS

The primary lesson learned by EPS was test test test! Problems experienced during flight could have been discovered and fixed earlier if more testing was performed before flight. Also, asking advice from knowledgeable sources would have improved the design from the beginning. The difficulty experienced with the MOSFETS might have been avoided if a mentor who understood more about MOSFETS was contacted earlier. During PCB design, it is important to have one common ground so all voltages are referenced off the same ground and are consistent; many pre-flight problems were due to misunderstanding this detail. Finally, using preexisting components allows for simpler and more functional designs.

E. CDH

The system could have been improved by applying the same formatting to file names as in the downlink format. The downlink format used UNIX time-stamps, while the pictures were saved under HH-MM-SS filenames, which produced a problem when we tried to synchronize the data with the pictures.

Also, the Raspberry Pi is a good option for this application except for the power restrictions. The Pi is current limited to 1.5 A which was exceeded when connecting both cameras, causing the Pi to enter a reboot loop. The solutions to this problem are not optimal, either requiring a USB hub, which can be sensitive or cause transmission problems, or patching it into the EPS board. Since only one camera was flown, this problem did not arise in flight, but was part of the reason only one camera was flown.

Finally, a far better backup system was required. The system in place could only replace the flight code in case of failure, but none of the packages or operating system configurations required for the flight code to be functional. The solution for this is to capture the complete state of the operating system in a stable state.

F. Thermal

Despite that the thermal system worked as well as was necessary, some improvements would be useful. Sensors on the payload monitored temperature of components throughout flight but no system was implemented to monitor those temperatures and cut power to components if they fell out of nominal temperature ranges which could help to prevent component damage. Additional temperature sensors should be implemented on multiple places on the baseplate to further characterize the effectiveness of the baseplate as a heat sink. In addition, the component that reached the highest temperature during flight, the motor driver, should also be heat sinked to the baseplate to minimize the possibility of the component overheating and malfunctioning.

V. Conclusion

Multiple images of the sun were captured in near hydrogen-alpha wavelength with HELIOS III's science camera. Because the system had to be fixed at a specific elevation and because the ADCS camera was not flown, the window of opportunity for taking images of the sun was vastly reduced. However, the majority of the images taken during the reduced time window contained images of the sun. This is a vast improvement upon the results of HELIOS I and II.

Unlike previous iterations of HELIOS, HELIOS III successfully tracked the sun throughout the entirety of flight. At only one point was it too far off from the sun to track, and this was quickly remedied with the use of a nudge command. With this minor exception, the tracking system functioned flawlessly, despite issues encounter immediately before flight. As illustrated in the plot of azimuth diode readings (Figure 20c)

and the elevation diode readings (Figure 20b on page 23, the system tracked the sun even when the sun was not at an optimal angle to be seen by the science camera.

The images taken of the sun were slightly off-center and out of focus and so did not capture any images of sunspots, but nonetheless proved the viability of solar tracking on a high altitude balloon platform.

Appendix

Team Demographics

Student	Gender	Ethnicity	Race	Student Status	Disability
Paige Arthur	Female	non-Hispanic	Caucasian	Undergraduate	No
Cooper Benson	Male	non-Hispanic	Caucasian	Undergraduate	No
Kristen Hanslik	Female	non-Hispanic	Caucasian	Undergraduate	No
Ryan Cutter	Male	non-Hispanic	Caucasian	Undergraduate	No
Brandon Boiko	Male	non-Hispanic	Caucasian	Undergraduate	No
Dylan Richards	Male	non-Hispanic	Caucasian	Undergraduate	No
Ryan Tabler	Male	non-Hispanic	Asian	Undergraduate	No
Alec Fiala	Male	non-Hispanic	Caucasian	Undergraduate	No
Chris Bradford	Male	non-Hispanic	Caucasian	Undergraduate	No
Mattia Astarita	Male	non-Hispanic	Caucasian	Undergraduate	No
Griffin Esposito	Male	non-Hispanic	Caucasian	Undergraduate	No
Jorge Cervantes	Male	Hispanic	Hispanic	Undergraduate	No
Matthew Haney	Male	non-Hispanic	Caucasian	Undergraduate	No
Justin Alvey	Male	non-Hispanic	Caucasian	Undergraduate	No
Tyler Lugger	Male	non-Hispanic	Caucasian	Undergraduate	No
Xiang Wang	Male	non-Hispanic	Asian	Undergraduate	No
Chris Rouw	Male	non-Hispanic	Caucasian	Undergraduate	No
Andrew Dudney	Male	non-Hispanic	Caucasian	Undergraduate	No
Anthony Lima	Male	non-Hispanic	Caucasian	Undergraduate	No
Caleb Lipscomb	Male	non-Hispanic	Caucasian	Undergraduate	No
Andrew McBride	Male	non-Hispanic	Caucasian	Undergraduate	No
Rebecca Lidvall	Female	non-Hispanic	Caucasian	Undergraduate	No
Flor Gordivas	Female	Hispanic	Hispanic	Undergraduate	No
Ashley Zimmerer	Female	non-Hispanic	Caucasian	Undergraduate	No

Structural Diagrams

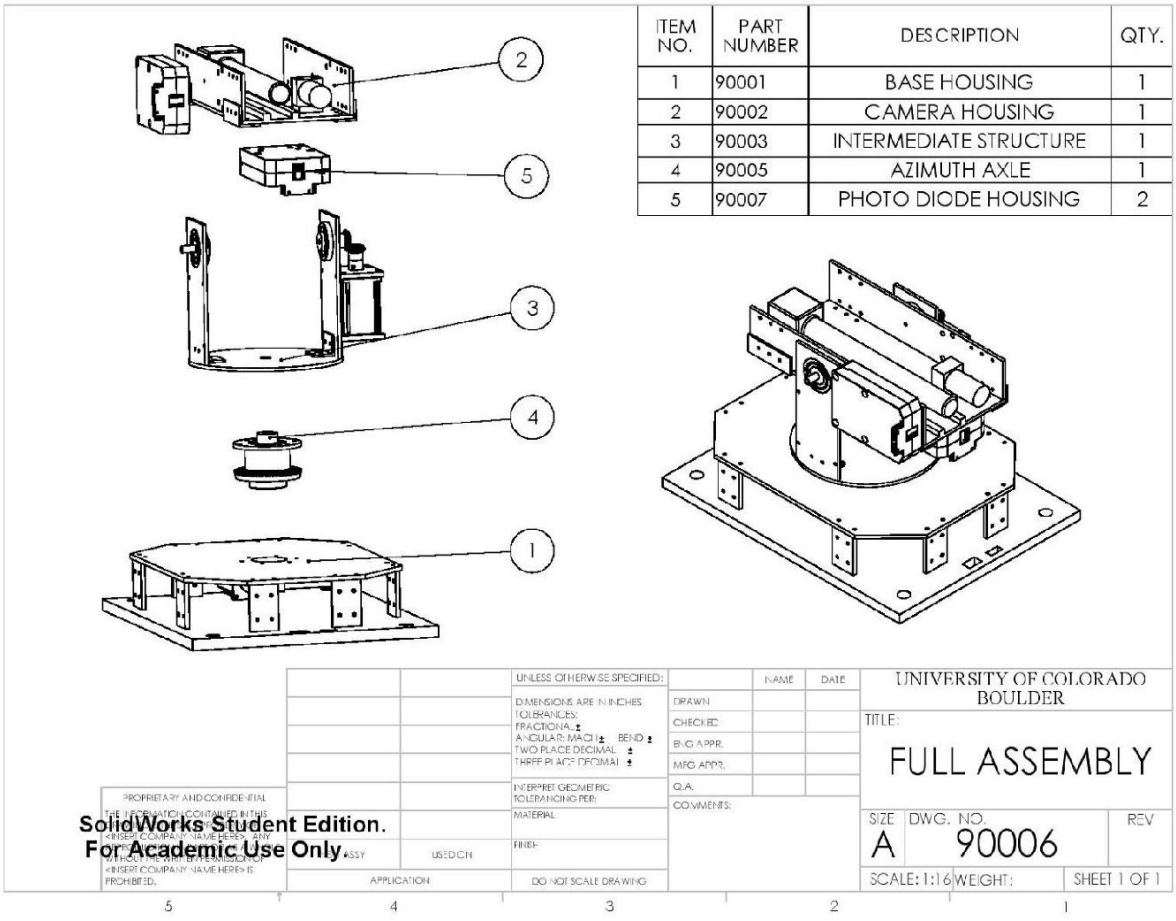

Figure 25: Bill of Materials (BOM) of full assembly

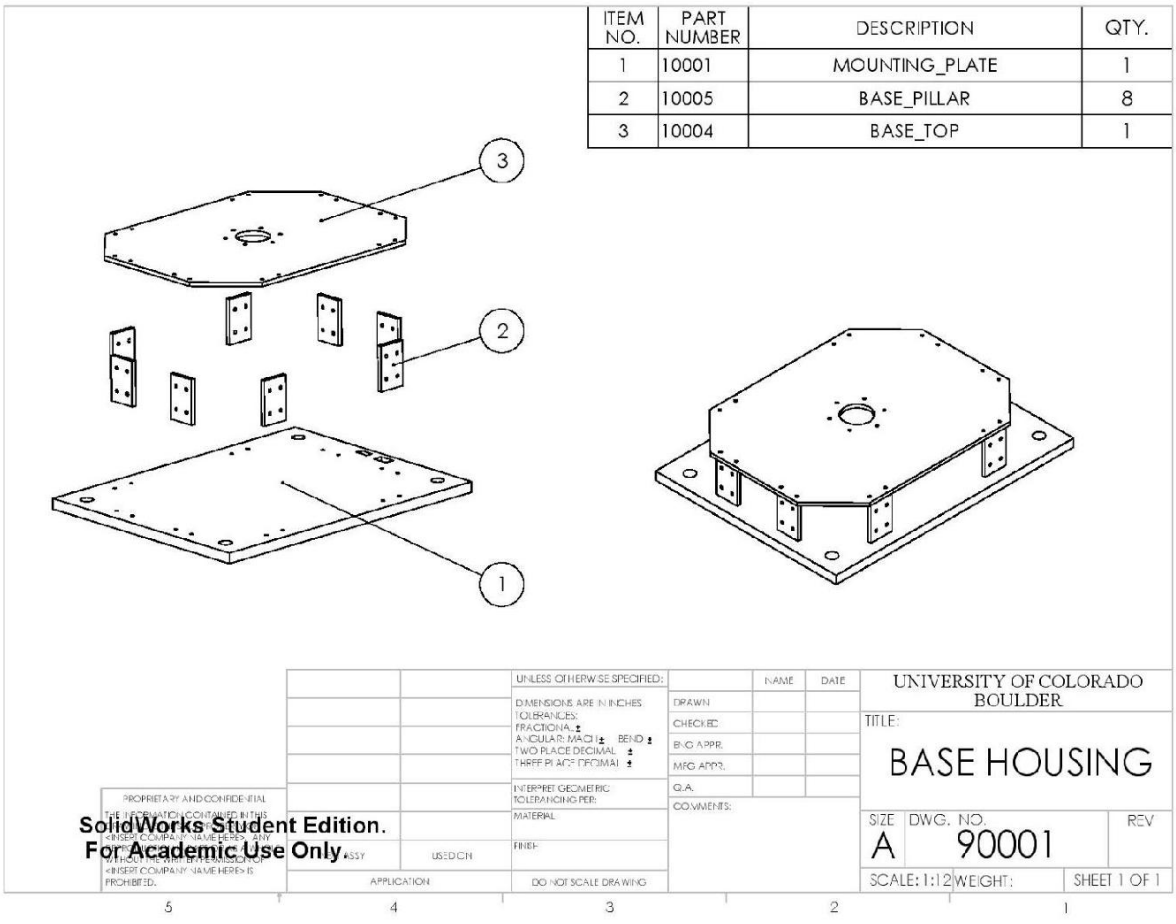

Figure 26: BOM of base housing. 3 main components:mounting plate, base pillar, base top.

ITEM NO.	PART NUMBER	DESCRIPTION	QTY.
1	20002	CAMERA_HOUSING_SIDE	2
2	00001	CAMERA HOUSING BRACKET	4
3	20001	CAMERA HOUSING BASE	1
4	80002	SCIENCE CAMERA	1
5	80001	ADCS CAMERA	1

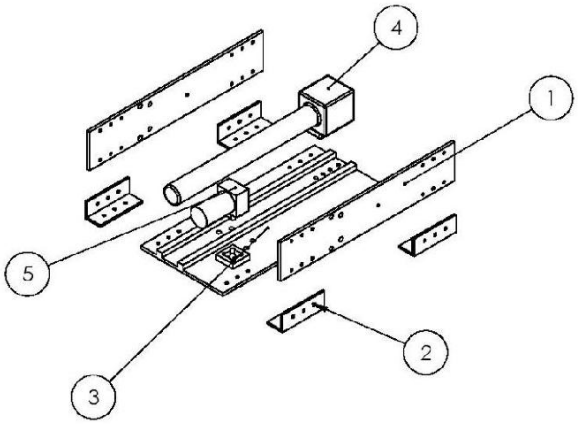

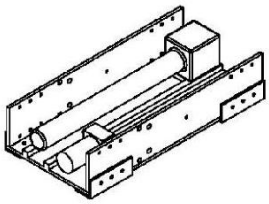

UNLESS OTHERWISE SPECIFIED:
DIMENSIONS ARE IN INCHES
TOLERANCES:
FRACTIONAL ±
ANGULAR: MACH ± BEND ±
TWO PLACE DECIMAL ±
THREE PLACE DECIMAL ±
INTERPRET GEOMETRIC TOLERANCING PER:
MATERIAL
FINISH
DO NOT SCALE DRAWING

	NAME	DATE
DRAWN		
CHECKED		
ENG APPR.		
MFG APPR.		
Q.A.		
COMMENTS:		

UNIVERSITY OF COLORADO BOULDER

TITLE: CAMERA HOUSING

SIZE A | DWG. NO. 90002 | REV

SCALE: 1:8 | WEIGHT: | SHEET 1 OF 1

Figure 27: BOM of camera housing with 5 major components.

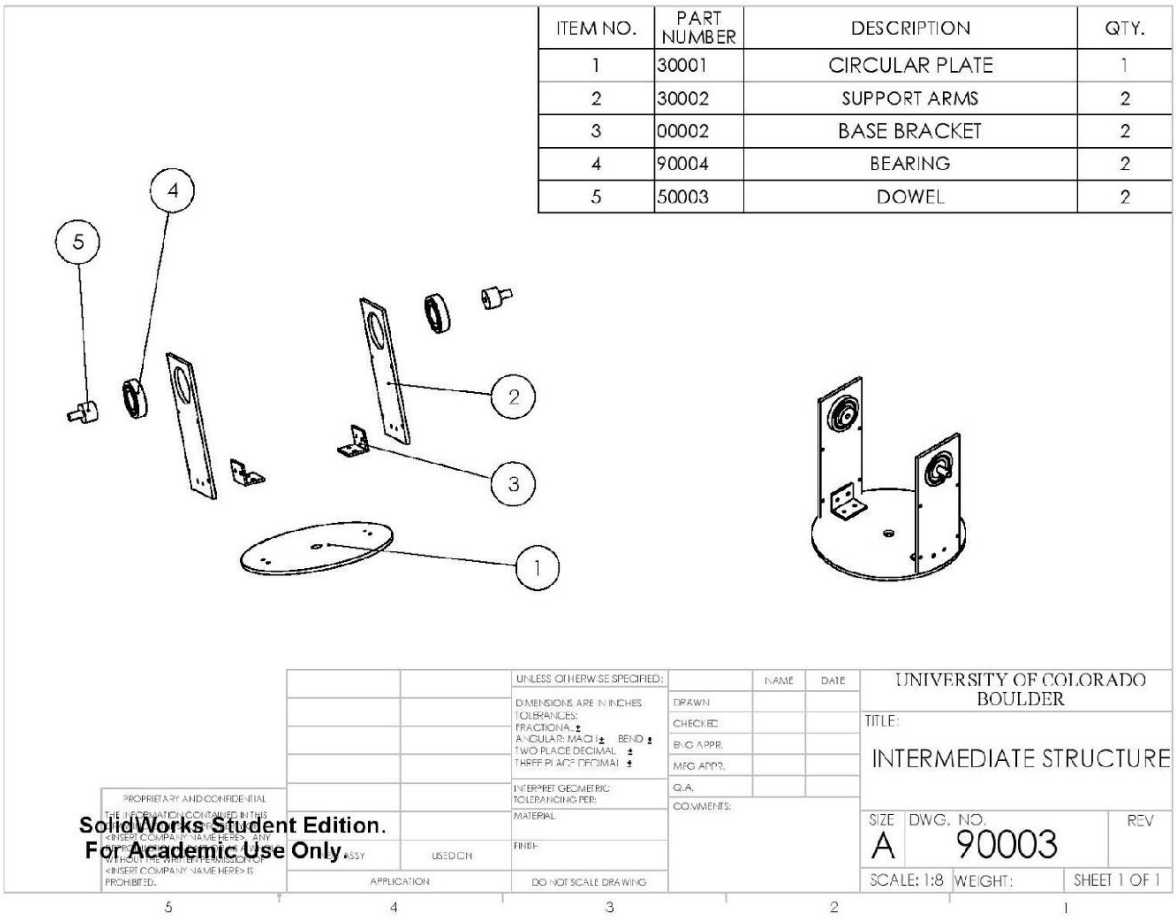

Figure 28: BOM of intermediate structure. This is what connects the base housing to the camera housing

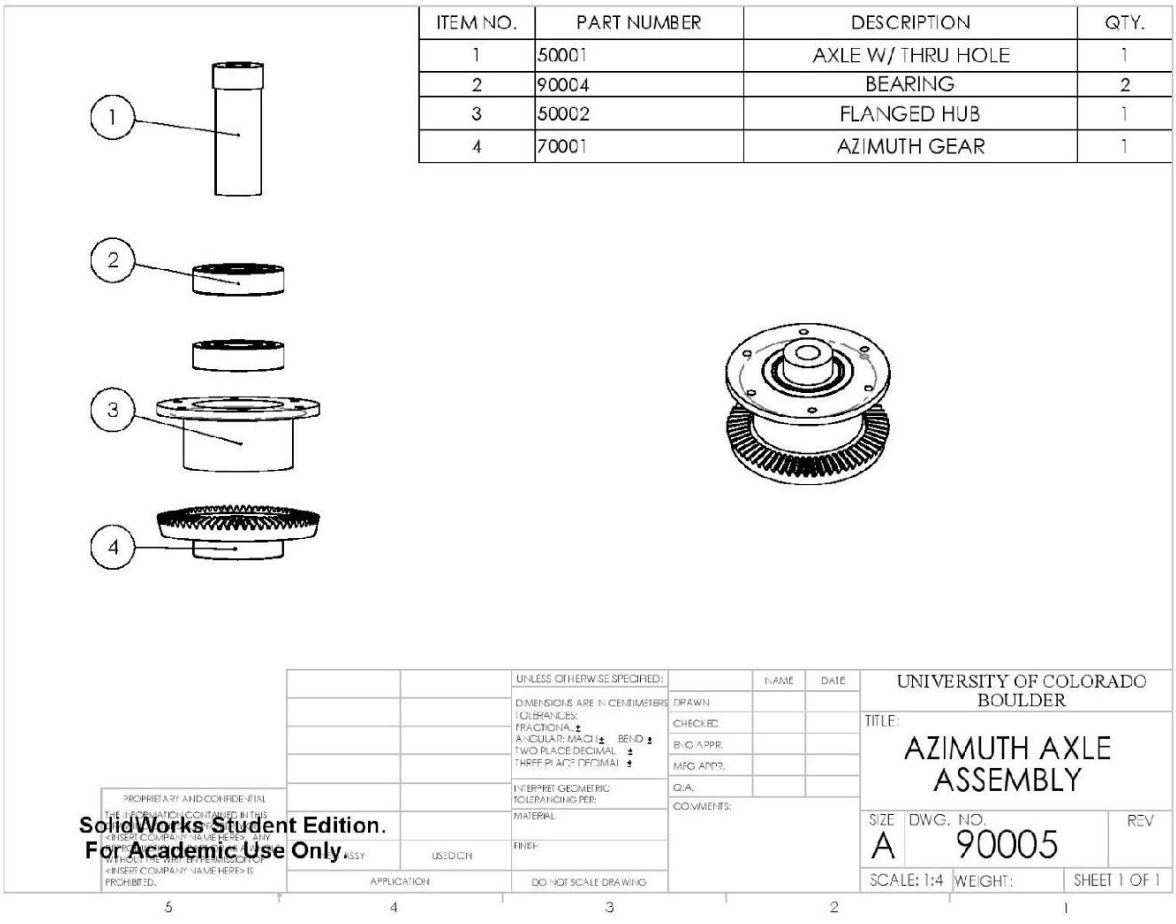

Figure 29: BOM of the azimuth axle.Bearings are spaced inside the hub.

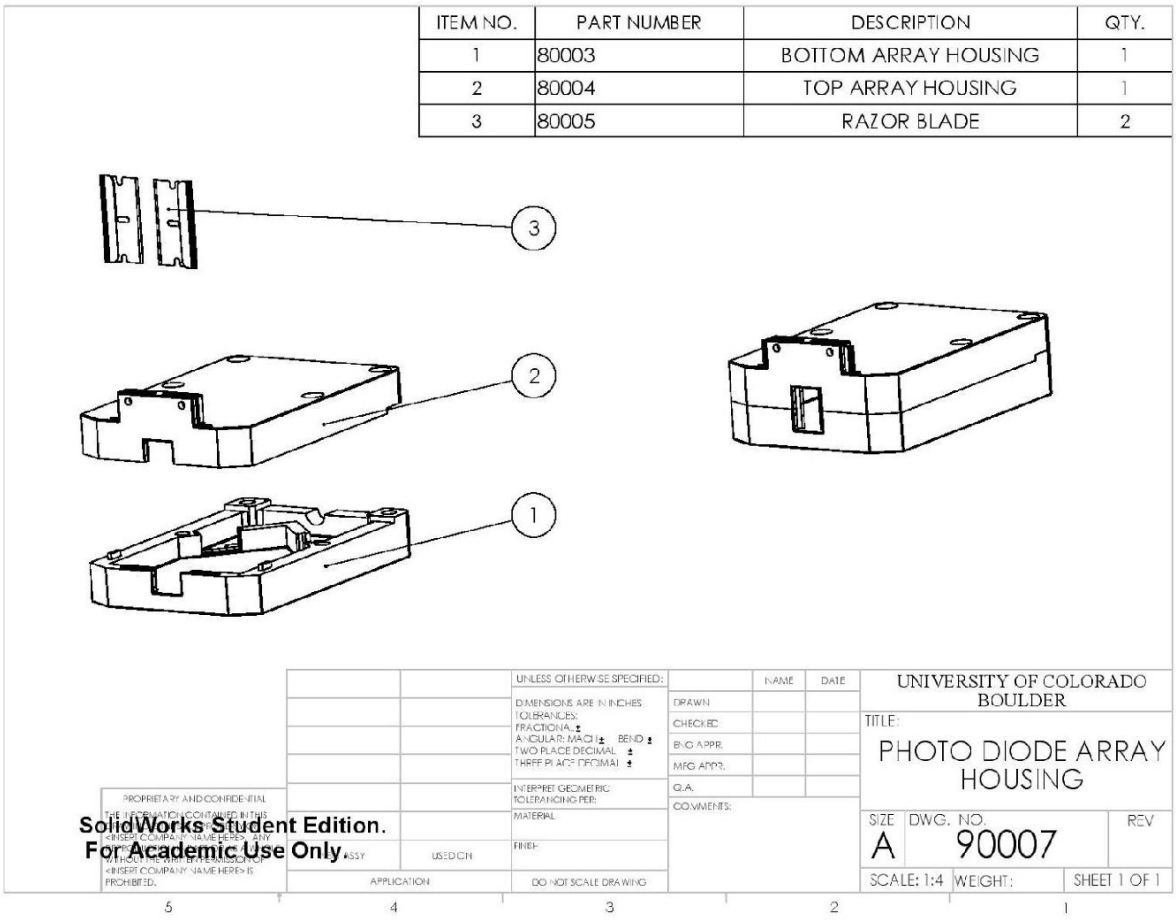

Figure 30: BOM of the photo diode housing.

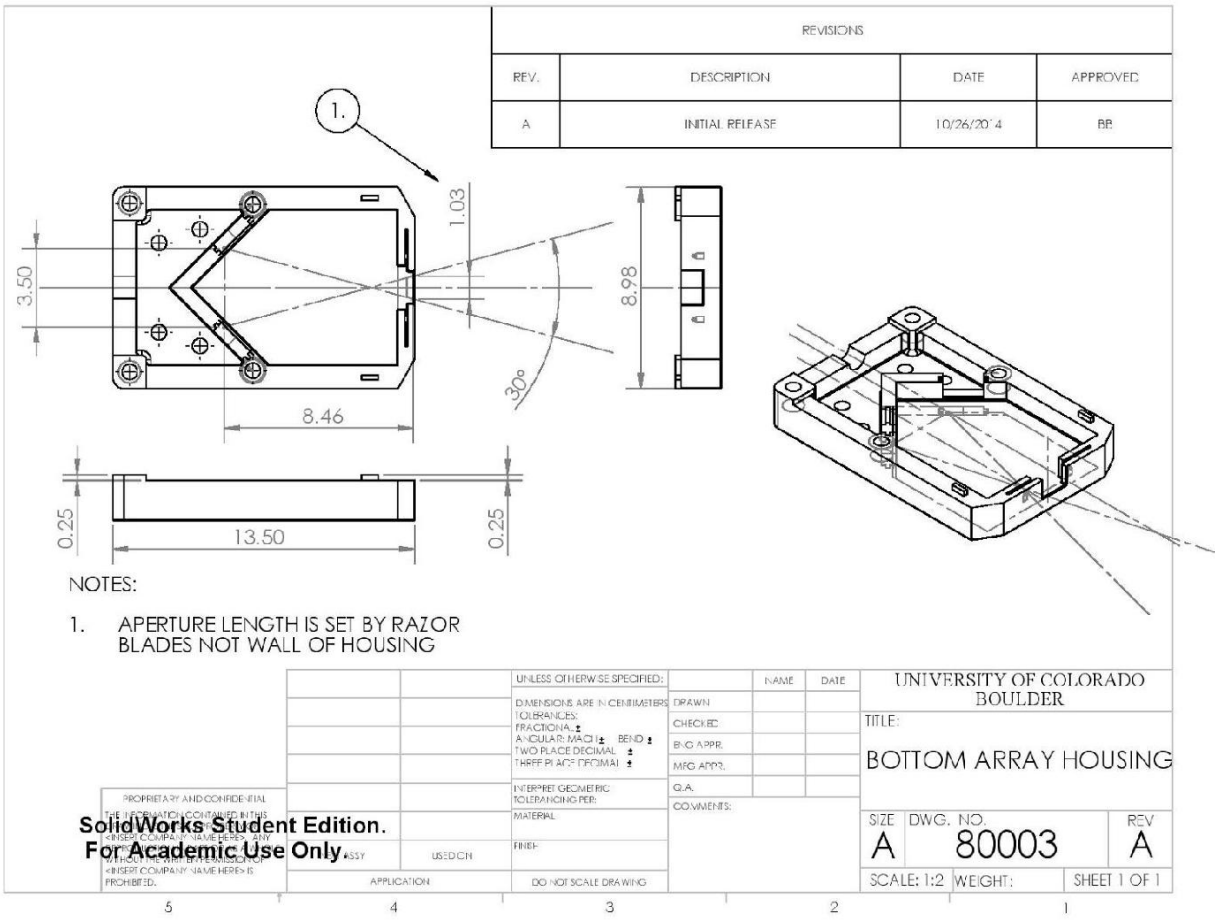

Figure 31: Detail of photo diode housings. Only shows dimensions for the baffling sketch.

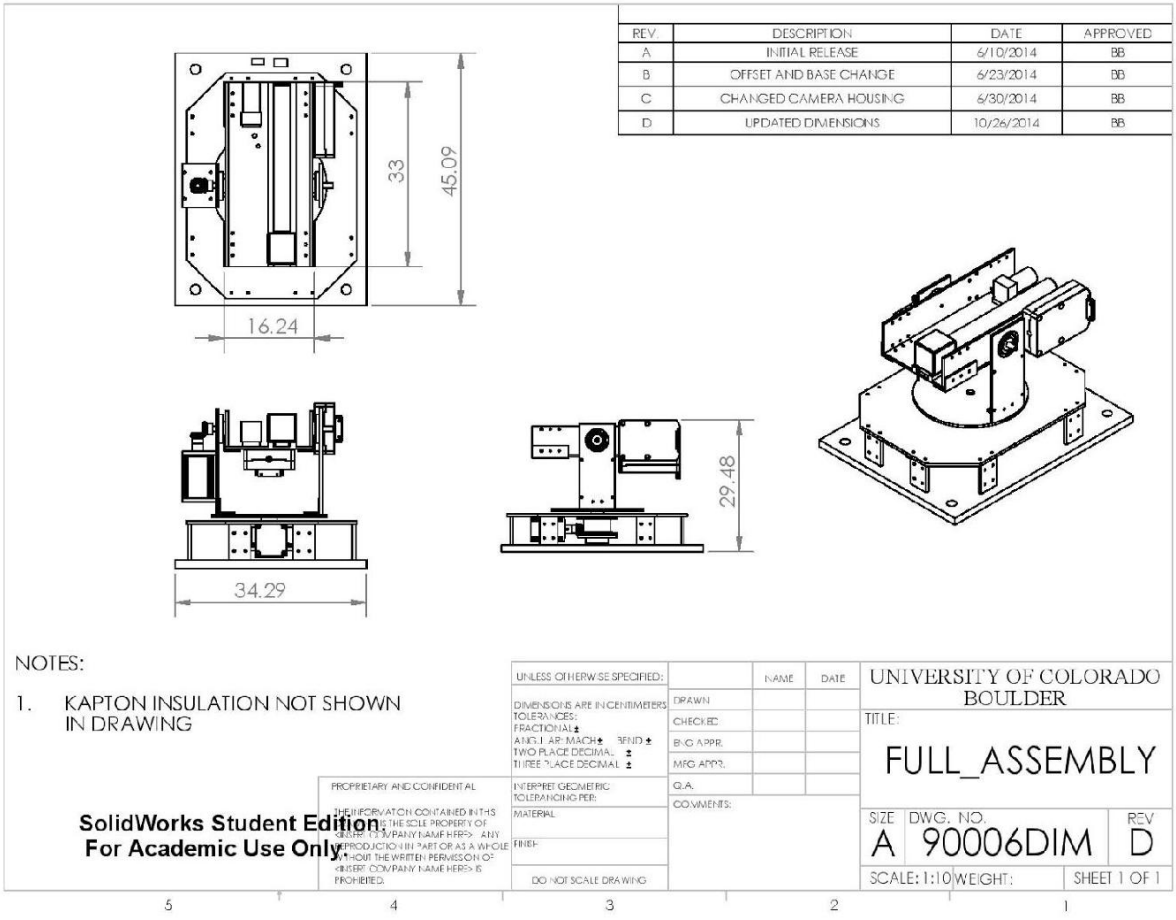

Figure 32: Basic dimensions for the full assembly, Over-all-height, Over-all-width, etc.

Acknowledgments

The team would like to thank the following people for their assistance with the project. HELIOS III's success would not have been possible without their help.

- Dr. Greg Guzik for his support of this mission over the past three iterations
- Doug Granger for his assistance before and during flight
- Mike Stewart for his work with the communications systems and pre-flight tests
- Jill Juneau for her electrical help at integration and flight
- Dr. James Green for his contributions to funding this project
- Lee Sutherland for the ballooning experience he provided
- Fabio Mezzalira for supporting the optics team
- Tim Spielman for machining complex parts for the structure
- Emily Brisnehan for her assistance with the thermal system
- Jesse Austin for his assistance with the photodiode and ADC boards
- Jesse Ellison for reviewing the EPS board designs before fabrication
- Chris Koehler for his unyielding support, advice, and confidence in the team
- The Engineering Excellence Fund and the Undergraduate Research Opportunity Program for generously funding this project
- The HELIOS II team for the excellent foundation that allowed this project to get off the ground

References

[1] Paige Arthur, Cooper Benson, Christopher Rouw, and Kristen Hanslik. The Potential for Solar Tracking and Observation On-board a High-Altitude Balloon Platform. April 2014.

[2] The Sun - Our Star. *Cool Cosmos - Multiwavelength Astronomy*, n.d.

[3] J. Eisenhamer. The Telescope - Hubble Essentials. *Hubblesite*, 2008.

[4] Observing the Sun in H-Alpha. *The Prairie Astronomy Club*, n.d.

[5] HELIOS II Team. Hydrogen-Alpha Exploration with Light Intensity Observation System (HELIOS) II Final Science Report. 2013.

[6] HELIOS III Team. Concept of design review. Presentation given at COSGC, February 2014.

[7] HELIOS III Team. Critical design review. Presentation given at COSGC, March 2014.

[8] HELIOS III Team. End of semester demonstration. Presentation given at COSGC, May 2014.

[9] HELIOS III Team. Final science presentation. Presentation given at COSGC, November 2014.

[10] HELIOS III Team. Preliminary data review. Presentation given at COSGC, September 2014.

[11] HELIOS III Team. Preliminary design review. Presentation given at COSGC, March 2014.